Numerical Simulation of a Continuously Measured Transmon Array

Taneli Tolppanen

MSc Thesis
Nano and Molecular Systems Research Unit
Theoretical Physics
University of Oulu
2022

Contents

1 Introduction **3**

2 Fundamentals of Measurement Theory **5**
2.1 The Measurement Postulate 5
2.1.1 Example: Application of the Measurement Postulate . . 5
2.2 Projective Measurements 6
2.3 Density Operator 7
2.4 General Quantum Measurements 7
2.4.1 Example: Weak Measurement 9

3 Continuous Measurement **11**
3.1 Quantum Jumps 11
3.1.1 Example: Photon detection of a Two Level Atom 14
3.2 The Wiener Increment and Itō calculus 16
3.3 Homodyne Detection 18
3.3.1 Example: $\hat{I}$ Quadrature Measurement of a Two Level Atom 22
3.4 Balanced Homodyne Detection 23
3.5 Heterodyne Detection 25

4 The Transmon Device and the Bose-Hubbard Model **28**
4.1 Superconductivity and the Josephson Junction 28
4.2 The Transmon Device 29
4.3 The Bose-Hubbard Model and the Transmon Chain 32

5 Heterodyne Detection of a System of Transmons **33**
5.1 Superconducting Cavity 33
5.2 Controlling a Transmon Qubit 34
5.3 Phase-Preserving Linear Amplifier 35
5.4 Heterodyne Detection of Transmons 37

6 Simulating Continuous Measurement With Julia **39**
6.1 Julia as a Programming Language 39
6.2 Solving Stochastic Differential Equations With the Differential Equations Package 40
6.2.1 Solving the Jump Problem 40
6.2.2 Solving Equations With Wiener Noise 42
6.2.3 Solving for Several Trajectories 44
6.2.4 Handling the Solution 44
6.3 Optimization Performance in Julia 46
6.4 Numerically Solving the Continuous Measurement Problems . . 48
6.4.1 Handling All the Parameters 48
6.4.2 Numerically Solving Quantum Jumps 48
6.4.3 Numerically Solving Homodyne Detection 49

6.4.4 Numerically Solving Heterodyne Detection 51
6.4.5 Performance of the Numerical Solutions 52

7 Example Observables for Continuously Measured Transmons 54
7.1 Boson Number of the Observed Site 55
7.2 Boson Number at the End of the Chain 56
7.3 Entanglement Entropy 58
7.4 Accuracy of the Results 59

8 Conclusions 61

Abstract

In this thesis continuous measurement is first introduced in the context of optical physics, and the derivation for the stochastic differential equations for quantum jumps, homodyne and heterodyne measurement is shown in outline. To study continuous measurement in superconducting circuits, the transmon device is introduced. The Bose-Hubbard model is used to model interacting transmons in an array. The circuit functionality needed for the measurement and control of transmons in a superconducting circuit is discussed. The stochastic master equation and the stochastic Schrödinger equation for the heterodyne measurement of transmons is provided. A guide for using the programming language Julia with the differential equations package to solve the continuous measurement problems is given, and the suitability of Julia for numerically simulating continuous measurement is examined. Julia is found to be efficient and a great tool for solving stochastic differential equations when used together with the differential equations package. To further demonstrate the capabilities of the numerical program implemented, we model five transmons, where the transmon in the middle is being continuously measured. We plot the boson number at the middle and at the end of the array. Furthermore, we plot the entanglement entropy between the first two and the last three transmons.

1 Introduction

Measurements are necessary to learn more about the fine details of nature. This thesis focuses on continuous measurements, in which information is extracted from a system continuously over a period of time. The theory of continuous measurements is applied for an array of transmons. The transmon is a superconducting circuit device, which can be used as a quantum bit. Continuously measured transmons are modeled with stochastic differential equations. These kind of equations can be difficult to solve analytically. Here, the programming language Julia is used to solve the stochastic differential equations. After reading the thesis, the reader is left with an intuitive understanding on how continuous measurement is derived and modeled. The reader will be familiar with the basics of superconductivity, and with the superconducting circuit elements used to control and measure transmons. The programming language Julia is introduced, so that the reader should feel confident in using it to solve the continuous measurement problems.

This thesis is in the field of quantum information and superconducting circuits. The potential of superconducting circuits for quantum information processing has been known for some time, but it is the recent years where there has been significant progress. Today it is possible to produce measurable and

controllable long-lived qubits. The continuous measurement of qubits enables quantum feedback, which is a crucial component for several quantum information processes, e.g. fault tolerant quantum computing. Further studying continuously measured transmons is a step toward a practical quantum computer. [1, 2]

The groundwork for understanding continuous measurement is laid in Chapter 2, where the measurement postulate is introduced, followed by projective measurement and an introduction to the density operator. Chapter 2 also introduces the idea of a probe, a separate system that interacts with the system that we are trying to measure, enabling the measurement of the target. Chapter 3 goes through the main ideas behind the derivation of the stochastic master equations, that depict quantum jumps, homodyne and heterodyne measurement. These continuous measurement problems are handled in the context of optical physics. To approach the continuous measurement of transmons, Chapter 4 gives an introduction to superconductivity and the transmon device. Multiple transmons interacting only with the neighboring transmon can be modeled with the Bose-Hubbard Hamiltonian, which is introduced at the end of Chapter 4. The circuitry that is typically found in superconducting circuits for controlling and measuring transmons is introduced in Chapter 5. Furthermore the superconducting cavity is presented, which is a crucial tool that enables both the measurement and the control of transmons. The concept of amplifying quantum mechanical signals is briefly discussed, followed by a depiction for what is needed for the heterodyne measurement of transmons. The Chapter 5 and the theory of this thesis is concluded by presenting the stochastic master equation and the stochastic Schrödinger equation used for modeling heterodyne measurement of transmons. Chapter 6 introduces the programming language Julia, which is used together with the differential equations package to solve the stochastic differential equations relating to the continuous measurement problems. A guide is given on how to use the differential equations package to solve the continuous measurement problems numerically. In Chapter 7 the code written in Chapter 6 is used to calculate the boson number of the transmons being measured, the boson number at the end of the array and the entanglement entropy between the first two and the last three transmons of the array. The thesis concludes with Chapter 8, where some ideas are given for expanding and improving the thesis.

2 Fundamentals of Measurement Theory

This chapter provides the tools needed to discuss continuous measurement. In this chapter the measurement postulate is introduced, followed by a brief look at projective measurements. To address situations where there are probabilities originating from the superposition, and probabilities due to lacking knowledge of the state of the system, the density operator is introduced. With these in mind, in the last chapter a more general picture for measurements in quantum mechanics is shown, by using a probe to realize the measurement of a given system.

2.1 The Measurement Postulate

In quantum mechanics, observable quantities are represented by Hermitian[1] operators $\hat{M}$. The eigenvalues $\{\lambda_m\}$ of the operator $\hat{M}$ are real and they correspond to possible measurement outcomes. The eigenstates $\{|m\rangle\}$ of the operator $\hat{M}$ form an orthonormal basis. With these eigenstates the state of the system $|\Psi\rangle$, which is a normalized complex vector, can be represented as

$$|\Psi\rangle = \sum_m c_m |m\rangle , \tag{2.1}$$

where $c_m = \langle m|\Psi\rangle$ and $\sum_m |c_m|^2 = 1$. The probability of getting the measurement result λ_m is $|\langle m|\Psi\rangle|^2 = |c_m|^2$ and the state of the system after the measurement is the corresponding eigenstate $|m\rangle$. This is called the measurement postulate. Here, and in the following chapters, it is assumed that the eigenvalues are discrete and non-degenerate. [3–5]

2.1.1 Example: Application of the Measurement Postulate

Consider that your friend is capable of preparing a system for you in some unknown quantum state $|\Psi\rangle$, and your task is to figure out what the quantum state specifically is. You have done measurements and you have found the measurement results to be either -1 or 1. Then according to the measurement postulate the eigenvalues $\{\lambda_m\}$ of the operator representing the measurement are $\lambda_0 = -1$ and $\lambda_1 = 1$. The matrix with these eigenvalues is the Pauli spin matrix

$$\hat{\sigma}_z = \begin{pmatrix} 1 & 0 \\ 0 & -1 \end{pmatrix} , \tag{2.2}$$

[1] If the operator $\hat{A}$ is Hermitian then $\hat{A} = \hat{A}^\dagger$.

and the eigenstates of this matrix are

$$|m := 0\rangle = |\downarrow\rangle = \begin{pmatrix} 0 \\ 1 \end{pmatrix}, \; |m := 1\rangle = |\uparrow\rangle = \begin{pmatrix} 1 \\ 0 \end{pmatrix}. \tag{2.3}$$

Comparing to Eq. (2.1), in the basis of these eigenstates the state of the system is

$$|\Psi\rangle = c_\downarrow |\downarrow\rangle + c_\uparrow |\uparrow\rangle , \tag{2.4}$$

with some unknown constants $c_\downarrow$ and $c_\uparrow$. Now let us say that you did several measurements and got the result $\lambda_1 = 1$ one-third of the time. Since the probability of getting the result is

$$|\langle\uparrow|\Psi\rangle|^2 = |c_\uparrow|^2 = \frac{1}{3}, \tag{2.5}$$

it follows that $c_\uparrow = \frac{1}{\sqrt{3}}$ and due to normalization $c_\downarrow = \sqrt{\frac{2}{3}}$. From this it follows that the quantum state of the system can be represented as

$$|\Psi\rangle = \sqrt{\frac{2}{3}} |\downarrow\rangle + \frac{1}{\sqrt{3}} e^{i\phi} |\uparrow\rangle , \tag{2.6}$$

for some phase ϕ. Realizations of this could be the measurement of spin or the measurement of the state of a qubit.

2.2 Projective Measurements

Coming from the measurement postulate the effect of a measurement $|\Psi\rangle \to |m\rangle$ is not very descriptive. To achieve a more mathematical picture, projective operators $\{\hat{P}_m\}$ can be defined. The Hermitian operator $\hat{M}$ can be diagonalized as

$$\hat{M} = \sum_m \lambda_m |m\rangle \langle m| , \tag{2.7}$$

so that in the basis of the eigenstates $\{|m\rangle\}$, the projective operators are

$$\hat{P}_m \equiv |m\rangle \langle m| . \tag{2.8}$$

The probability p_m of getting the measurement result λ_m is

$$p_m = \langle\Psi| \hat{P}_m^\dagger \hat{P}_m |\Psi\rangle = \langle\Psi| \hat{P}_m |\Psi\rangle = |\langle m|\Psi\rangle|^2, \tag{2.9}$$

and the state of the system after the measurement is

$$|\Psi\rangle \to \frac{\hat{P}_m |\Psi\rangle}{\sqrt{p_m}}. \tag{2.10}$$

The types of measurements presented here and in the previous chapter are called von Neumann measurements. [6, 7]

2.3 Density Operator

The density operator $\hat{\rho}$, or the density matrix, can be used to describe the system when we simply do not know in which state the system is [5]. Consider that we know that the system is in the state $|\Psi\rangle$, then the corresponding density operator is

$$\hat{\rho} = |\Psi\rangle \langle\Psi| . \tag{2.11}$$

Now if we do not know in which state the system is, instead we know that it is in the state $|\Psi_1\rangle$ with the probability $p_1 = 0.4$ or in the state $|\Psi_2\rangle$ with the probability $p_2 = 0.6$, then the corresponding density operator is

$$\hat{\rho} = 0.4 |\Psi_1\rangle \langle\Psi_1| + 0.6 |\Psi_2\rangle \langle\Psi_2| . \tag{2.12}$$

This type of states are called mixed. The type of states as in Eq. (2.11) are called pure. Analogous to Eq. (2.12) the density operator can be a mixture of any number of states $\hat{\rho} = \sum_i p_i |\Psi_i\rangle \langle\Psi_i|$, with each having a probability of p_i. The trace of the density operator is the sum of the probabilities of finding it in any of the possible states, thus for every valid density operator $\mathrm{Tr}(\hat{\rho}) = 1$. This is somewhat analogous to the norm of the state vector being equal to one. The purity of a given density operator can be calculated as $\mathrm{Tr}(\hat{\rho}^2) \in [0, 1]$, where one is equal to the state being completely pure. For the following chapters we need the density operator versions of the projective measurement equations from the previous chapter. To handle mixed states, equation (2.9) becomes

$$p_m = \mathrm{Tr}\left(\hat{P}_m \hat{\rho} \hat{P}_m^\dagger\right), \tag{2.13}$$

and equation (2.10)

$$\hat{\rho} \to \frac{\hat{P}_m \hat{\rho} \hat{P}_m^\dagger}{p_m}. \tag{2.14}$$

With these tools we are ready to discuss measurement via a probe. [5, 7]

2.4 General Quantum Measurements

In practice the quantum system of interest is never directly measured. To measure it a separate system is needed. This separate system works as the measurement device. Von Neumann measurements do not describe every possible measurement and applying them directly to the system of interest might not yield correct results. Nevertheless, they can be used to derive all other types of measurements. In the following, the system of interest will be referred to simply as the system, as long as there is no risk of confusion, and the measurement device will be referred to as the probe. To describe more general measurements, the interaction between these two systems is needed.

Before the system and the probe are brought into contact, the system and the probe are assumed to be in the states $\hat{\rho}_{\mathrm{S}}$ and $\hat{\rho}_{\mathrm{P}}$ respectively. The initial state $\hat{\rho}_{\mathrm{I}}$ of the combined system is

$$\hat{\rho}_{\mathrm{I}} = \hat{\rho}_{\mathrm{P}} \otimes \hat{\rho}_{\mathrm{S}}. \tag{2.15}$$

These two system are allowed to interact for some period of time. This interaction is described by some unitary operator $\hat{U}$. After the interaction, the states of the probe are correlated with the states of the system. Now the state of the combined system is

$$\hat{\rho}_{\mathrm{U}} = \hat{U}\hat{\rho}_{\mathrm{I}}\hat{U}^{\dagger} = \hat{U}\left(\hat{\rho}_{\mathrm{P}} \otimes \hat{\rho}_{\mathrm{S}}\right)\hat{U}^{\dagger}. \tag{2.16}$$

Due to the correlation it is possible to obtain information of the system of interest by doing a projective measurement on the probe. This projective measurement is done in a basis state $|n\rangle$ of the probe. The projective measurement concludes the measurement of the system of interest, and after this, by using Eq. (2.14), the state of the combined system is

$$\hat{\rho}_{\mathrm{M}} = \left(|n\rangle\langle n| \otimes \hat{I}\right)\hat{\rho}_{\mathrm{U}}\left(|n\rangle\langle n| \otimes \hat{I}\right) \tag{2.17}$$

$$= \left(|n\rangle\langle n| \otimes \hat{I}\right)\hat{U}\left(\hat{\rho}_{\mathrm{P}} \otimes \hat{\rho}_{\mathrm{S}}\right)\hat{U}^{\dagger}\left(|n\rangle\langle n| \otimes \hat{I}\right). \tag{2.18}$$

Notice that for convenience the normalization has been dropped out.

To proceed, it can be noted that since there are no restrictions on the unitary operator $\hat{U}$, the initial state of the probe can be chosen to be $\hat{\rho}_{\mathrm{P}} = |0\rangle\langle 0|$. The unitary operator can be presented as

$$\hat{U} = \sum_{nn'} |n\rangle\langle n'| \otimes \hat{A}_{nn'}, \tag{2.19}$$

where $\hat{A}_{nn'}$ are operators acting on the system of interest. Since $\hat{U}$ is a unitary operator, we find that

$$\hat{I} \otimes \hat{I} = \hat{U}^{\dagger}\hat{U} = \left(\sum_{nn'} |n\rangle\langle n'| \otimes \hat{A}^{\dagger}_{n'n}\right)\left(\sum_{mm'} |m\rangle\langle m'| \otimes \hat{A}_{mm'}\right) \tag{2.20}$$

$$= \sum_{nn'm'} |n\rangle\langle m'| \otimes \hat{A}^{\dagger}_{n'n}\hat{A}_{n'm'} \tag{2.21}$$

$$= \sum_{ij} |i\rangle\langle j| \otimes \sum_{n} \hat{A}^{\dagger}_{ni}\hat{A}_{nj}. \tag{2.22}$$

Due to the equality with identity, it has to be so that $\sum_n \hat{A}^{\dagger}_{ni}\hat{A}_{nj} = \hat{I}\delta_{ij}$. The state of the combined system after the measurement is

$$\hat{\rho}_{\mathrm{M}} = \left(|n\rangle\langle n| \otimes \hat{I}\right)\hat{U}\left(|0\rangle\langle 0| \otimes \hat{\rho}_{\mathrm{S}}\right)\hat{U}^{\dagger}\left(|n\rangle\langle n| \otimes \hat{I}\right) \tag{2.23}$$

$$= \left(\sum_{n'} |n\rangle\langle n'| \otimes \hat{A}_{nn'}\right)\left(|0\rangle\langle 0| \otimes \hat{\rho}_{\mathrm{S}}\right)\left(\sum_{m'} |m'\rangle\langle n| \otimes \hat{A}^{\dagger}_{nm'}\right) \tag{2.24}$$

$$= |n\rangle\langle n| \otimes \hat{A}_{n0}\hat{\rho}_{\mathrm{S}}\hat{A}^{\dagger}_{n0}. \tag{2.25}$$

Now we see that due to the initial state of the probe, the only relevant operators are $\hat{A}_{n0} \equiv \hat{A}_n$. These operators are restricted by the rule from above, so that $\sum_n \hat{A}_n^\dagger \hat{A}_n = \hat{I}$. We also see that the normalized state of the system, after observing the probe to be in the state $|n\rangle$, is

$$\hat{\rho}_n = \frac{\hat{A}_n \hat{\rho}_\mathrm{S} \hat{A}_n^\dagger}{\mathrm{Tr}\left(\hat{A}_n \hat{\rho}_\mathrm{S} \hat{A}_n^\dagger\right)}. \tag{2.26}$$

Using Eq. (2.13), the probability of observing the probe to be in this state after the interaction is

$$\begin{aligned} p_n &= \mathrm{Tr}\left(\left(|n\rangle\langle n| \otimes \hat{I}\right)\hat{\rho}_\mathrm{U}\left(|n\rangle\langle n| \otimes \hat{I}\right)\right) = \mathrm{Tr}\left(\hat{\rho}_\mathrm{M}\right) && (2.27)\\ &= \mathrm{Tr}\left(|n\rangle\langle n| \otimes \hat{A}_n \hat{\rho}_\mathrm{S} \hat{A}_n^\dagger\right) = \mathrm{Tr}\left(|n\rangle\langle n|\right)\mathrm{Tr}\left(\hat{A}_n \hat{\rho}_\mathrm{S} \hat{A}_n^\dagger\right) && (2.28)\\ &= \mathrm{Tr}\left(\hat{A}_n \hat{\rho}_\mathrm{S} \hat{A}_n^\dagger\right). && (2.29) \end{aligned}$$

General quantum measurements are described by an interaction between the probe and the system of interest. For every set of operators $\{\hat{A}_n\}$ that satisfies the rule $\sum_n \hat{A}_n^\dagger \hat{A}_n = \hat{I}$, it is possible to devise a probe that realizes this interaction, at least in theory. The state of the system, after the projective measurement of the probe, is given by Eq. (2.26), and the probability for this by Eq. (2.27). The operators $\hat{A}_n$ are called the measurement operators or the Kraus operators. [5,7]

2.4.1 Example: Weak Measurement

Consider a qubit that is initially in the mixed state $\hat{\rho} = 1/2\left(|0\rangle\langle 0| + |1\rangle\langle 1|\right)$. Then consider the set of operators $\{\hat{A}_0, \hat{A}_1\}$

$$\hat{A}_0 = \sqrt{\epsilon}\,|0\rangle\langle 0| + \sqrt{1-\epsilon}\,|1\rangle\langle 1| = \begin{pmatrix} \sqrt{\epsilon} & 0 \\ 0 & \sqrt{1-\epsilon} \end{pmatrix}, \tag{2.30}$$

$$\hat{A}_1 = \sqrt{1-\epsilon}\,|0\rangle\langle 0| + \sqrt{\epsilon}\,|1\rangle\langle 1| = \begin{pmatrix} \sqrt{1-\epsilon} & 0 \\ 0 & \sqrt{\epsilon} \end{pmatrix}, \tag{2.31}$$

so that

$$\hat{A}_0^\dagger \hat{A}_0 + \hat{A}_1^\dagger \hat{A}_1 = |0\rangle\langle 0| + |1\rangle\langle 1| = \hat{I}. \tag{2.32}$$

Therefore these operators are possible measurement operators. Finding the unitary operator that realizes these operators is not necessary. Using Eq. (2.26), the state of the system after observing the measurement result 0 is

$$\hat{\rho}_0 = \frac{\hat{A}_0 \hat{\rho} \hat{A}_0^\dagger}{\mathrm{Tr}\left(\hat{A}_0 \hat{\rho} \hat{A}_0^\dagger\right)} = \begin{pmatrix} \epsilon & 0 \\ 0 & 1-\epsilon \end{pmatrix}. \tag{2.33}$$

To see how mixed the state is, the purity can be calculated:

$$\mathrm{Tr}\left(\hat{\rho}_0^2\right) = \epsilon^2 + (1-\epsilon)^2\,, \tag{2.34}$$

which has been plotted in Fig. 1. For $\epsilon = 1/2$ the measurement does not change the initial state, since then the measurement does not yield any useful information. For $\epsilon \in \{0, 1\}$ the measurement acts as a projective measurement, as in Chapter 2.2. After this we completely know the state of the qubit. These kind of measurements are a type of strong measurements. For $\epsilon \in (1/2, 1)$ the measurement does not completely remove the uncertainty in the state. Measurements for which $\epsilon \approx 1/2$ are a type of a weak measurement. [5, 6]

The types of measurements presented in Chapter 2.4 are often called positive operator valued measures or POVMs. They are not the most general type of a measurement. What can still be added to this is the classical uncertainty in the measurement result or uncertainty in what measurement was made. For this master's thesis these type of measurement are not needed. The reader, if interested, can read more about them in Chapter 1.6 of reference [5] and Chapter 1.4 of reference [7].

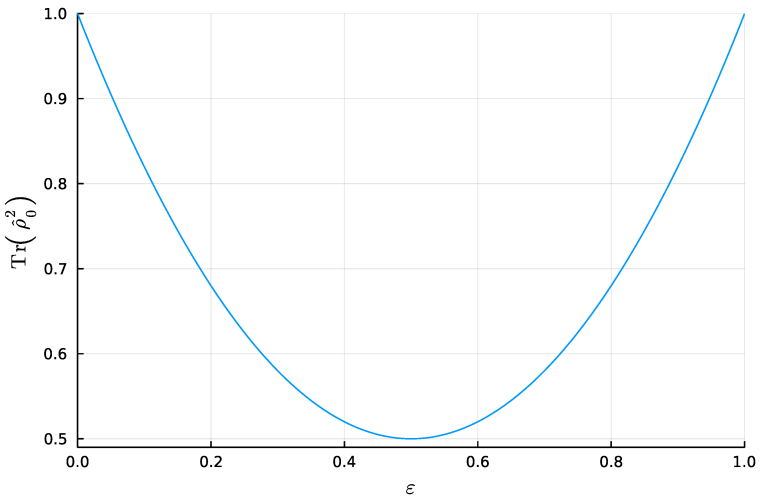

Figure 1: The purity of the state $\hat{\rho}_0$ of Eq. (2.33) as a function of ϵ. The state after the measurement is completely pure only if $\epsilon \in \{0, 1\}$.

3 Continuous Measurement

The measurements in the previous chapter affected the system of interest for a single moment in time. In practice every measurement takes some time to be completed. This chapter gives an introduction to measurements that extract information out of the system over a period of time. These types of measurements are called continuous measurements. The different kinds of continuous measurements that will be introduced in this chapter are counting the photons emitted from a system, homodyne detection, balanced homodyne detection and heterodyne detection. Later we will be interested in the heterodyne measurement of transmons, so the role of the other continuous measurement types is to lead up to heterodyne detection. The goal is to provide the stochastic differential equations that simulate these measurements, and to give an intuitive understanding for how these equations are derived. A short introduction to Itō calculus is given, and how it is used in dealing with stochastic differential equations is demonstrated. Measurements are a way to gain information about the state of a system, but they also have an effect on it, and as such are a way to manipulate the system. Here the interest lies in how the quantum system reacts to it being measured.

3.1 Quantum Jumps

Discontinuous changes in the evolution of the system due to continuous measurement are characteristic for quantum jumps. This abrupt change in the state of the system follows, from example, when counting the photons emitted from a system. The times when the photons are emitted is random by nature, so the evolution of the system is described by differential equations that have a random component. This random component is called noise. The noise can be realized in infinite many ways, and thus there exists infinite many solutions to the given problem. A single solution to this type of a differential equation is called a trajectory and these type of differential equations are called stochastic differential equations. Quantum jumps are not limited to photon counting. To not lose generality, the emitting of a photon can be thought of as an event, and the counting of photons is then counting of events. In this chapter the differential equation for counting of events will be provided, followed by an example of counting the photons emitted by a two-level atom. This chapter follows closely the Chapter 3.3 of Ref. [5].

Generally speaking, the probability that an event occurs in a time interval dt can be defined to be λdt, where λ is called the probability rate. Then the probability that the event does not occur is $1 - \lambda dt$. These events can be

counted by introducing the random variable $N(t)$ that gives the integer number of events that have occurred in the time t. $N(t)$ can also be referred to as a counting process. Since in every time interval there can occur only one event, the increment of $N(t)$, dN, has two possible values: $dN = 0$ or $dN = 1$. From this it follows that $dN^2 = dN$. Now the probability that $dN = 1$ in a given interval is just the probability that an event occurs: $\mathrm{Prob}[dN = 1] = \lambda dt$. Similarly $\mathrm{Prob}[dN = 0] = 1 - \lambda dt$.

The system needs to be measured for us to be able to count the possible events. So for us to be able to count the events, we need to do a measurement in every time-step dt. This measurement has two possible outcomes: we see that an event occurred or that it did not. This implies that the outcomes correspond to two measurement operators. Let $\hat{A}_1$ be the operator that corresponds to the outcome that an event occurred, and $\hat{A}_0$ correspond to the outcome that no event occurred. From the previous chapter, we see that the probability that we observe the measurement outcome to be the one relating to the measurement operator $\hat{A}_1$, is given by Eq. (2.13). This has to agree with the probability of the event occurring:

$$\mathrm{Tr}\left(\hat{A}_1 \hat{\rho} \hat{A}_1^\dagger\right) = \lambda dt. \tag{3.1}$$

For the left hand side to be proportional to dt, $\hat{A}_1$ has to be proportional to $\sqrt{dt}$. So let's choose $\hat{A}_1 = \hat{\Omega}\sqrt{dt}$, where $\hat{\Omega}$ is some constant operator. Since $\hat{A}_0$ and $\hat{A}_1$ are measurement operators, they have to obey they rule $\hat{A}_0^\dagger \hat{A}_0 + \hat{A}_1^\dagger \hat{A}_1 = \hat{I}$. From this it follows that

$$\hat{A}_0^\dagger \hat{A}_0 = \hat{I} - \hat{\Omega}^\dagger \hat{\Omega} dt. \tag{3.2}$$

Now setting $\hat{A}_0 = \hat{I} + \hat{X}dt$, inserting it to the equation above and expanding to the first order in dt, we end up with

$$\left(\hat{I} + \hat{X}^\dagger dt\right)\left(\hat{I} + \hat{X}dt\right) = \hat{I} + \left(\hat{X}^\dagger + \hat{X}\right)dt = \hat{I} - \hat{\Omega}^\dagger \hat{\Omega} dt. \tag{3.3}$$

So $\hat{X}^\dagger + \hat{X} = -\hat{\Omega}^\dagger \hat{\Omega}$. Since $\hat{\Omega}^\dagger \hat{\Omega}$ is hermitian, $\hat{X}$ can also be chosen to be hermitian, and we end up with

$$\hat{X} = -\frac{\hat{\Omega}^\dagger \hat{\Omega}}{2}. \tag{3.4}$$

Using this, we see that the proper measurement operators are

$$\hat{A}_1 = \hat{\Omega}\sqrt{dt}, \tag{3.5}$$

$$\hat{A}_0 = \hat{I} - \frac{\hat{\Omega}^\dagger \hat{\Omega}}{2} dt, \tag{3.6}$$

for some constant operator $\hat{\Omega}$. Inserting $\hat{A}_1$ to Eq. (3.1), we also see that the probability rate, also referred to as the instantaneous rate of counts, is given by

$$\lambda = \mathrm{Tr}\left(\hat{\Omega}\hat{\rho}\hat{\Omega}^\dagger\right) = \left\langle \hat{\Omega}^\dagger \hat{\Omega} \right\rangle. \tag{3.7}$$

The last thing to derive is how the state of the system changes as the events are being recorded. If there is no event, the state of the system is given by the measurement operator $\hat{A}_0$ and Eq. (2.26) to the first order in dt:

$$\hat{\rho} \to \hat{\rho}' = \frac{\hat{A}_0 \hat{\rho} \hat{A}_0^\dagger}{\left\langle \hat{A}_0^\dagger \hat{A}_0 \right\rangle} \tag{3.8}$$

$$= \frac{\left(\hat{I} - \frac{\hat{\Omega}^\dagger \hat{\Omega}}{2} dt\right) \hat{\rho} \left(\hat{I} - \frac{\hat{\Omega}^\dagger \hat{\Omega}}{2} dt\right)}{\left\langle \left(\hat{I} - \frac{\hat{\Omega}^\dagger \hat{\Omega}}{2} dt\right)^2 \right\rangle} \tag{3.9}$$

$$= \frac{\hat{\rho} - \left(\frac{\hat{\Omega}^\dagger \hat{\Omega}}{2} \hat{\rho} + \hat{\rho} \frac{\hat{\Omega}^\dagger \hat{\Omega}}{2}\right) dt}{1 - \left\langle \hat{\Omega}^\dagger \hat{\Omega} \right\rangle dt} \tag{3.10}$$

$$= \left(\hat{\rho} - \left(\frac{\hat{\Omega}^\dagger \hat{\Omega}}{2} \hat{\rho} + \hat{\rho} \frac{\hat{\Omega}^\dagger \hat{\Omega}}{2}\right) dt\right) \left(1 + \left\langle \hat{\Omega}^\dagger \hat{\Omega} \right\rangle dt\right) \tag{3.11}$$

$$= \hat{\rho} + \left(\left\langle \hat{\Omega}^\dagger \hat{\Omega} \right\rangle \hat{\rho} - \frac{1}{2} \left\{ \hat{\Omega}^\dagger \hat{\Omega}, \hat{\rho} \right\}\right) dt. \tag{3.12}$$

Here on line (3.10) in the denominator the relation $1/(1-x) = 1 + x + x^2 ...$ was used, and $\{\hat{A}, \hat{B}\} = \hat{A}\hat{B} + \hat{B}\hat{A}$ is the anticommutator. Similarly if the event occurs the state is given by

$$\hat{\rho} \to \hat{\rho}' = \frac{\hat{\Omega} \hat{\rho} \hat{\Omega}^\dagger}{\left\langle \hat{\Omega}^\dagger \hat{\Omega} \right\rangle} \tag{3.13}$$

Since these changes happen in every time interval dt, this implies that $\hat{\rho}' = \hat{\rho} + d\hat{\rho}$. In the case of no event occurring we find that

$$d\hat{\rho} = \left(\left\langle \hat{\Omega}^\dagger \hat{\Omega} \right\rangle \hat{\rho} - \frac{1}{2} \left\{ \hat{\Omega}^\dagger \hat{\Omega}, \hat{\rho} \right\}\right) dt, \tag{3.14}$$

and in the case of the event occurring

$$d\hat{\rho} = \frac{\hat{\Omega} \hat{\rho} \hat{\Omega}^\dagger}{\left\langle \hat{\Omega}^\dagger \hat{\Omega} \right\rangle} - \hat{\rho}. \tag{3.15}$$

If we take a look at Eq. (3.14), we see that in the case of no event occurring, the change in the state of the system is infinitesimal. This is comparable to a weak measurement. When an event occurs, we see from Eq. (3.15) that it compares to a strong measurement. The probability that an event occurs is given by $\lambda dt = \left\langle \hat{\Omega}^\dagger \hat{\Omega} \right\rangle dt$, so that in every time-step it is more likely for the event to not occur. From these we can piece together that the evolution of the state is continuous until an event occurs. When an event does occur the effect of it is an abrupt and discontinuous change in the state of the system. The

system jumps from one state to another. Moving forward, we can combine these equations to form the differential equation for quantum jumps. By using dN, that is $dN = 1$ when an event occurs and zero otherwise, we find the following differential equation

$$d\hat{\rho} = -\frac{i}{\hbar}\left[\hat{H},\hat{\rho}\right]dt + (1-dN)\left(\left\langle\hat{\Omega}^\dagger\hat{\Omega}\right\rangle\hat{\rho} - \frac{1}{2}\left\{\hat{\Omega}^\dagger\hat{\Omega},\hat{\rho}\right\}\right)dt + \left(\frac{\hat{\Omega}\hat{\rho}\hat{\Omega}^\dagger}{\left\langle\hat{\Omega}^\dagger\hat{\Omega}\right\rangle} - \hat{\rho}\right)dN \tag{3.16}$$

$$= -\frac{i}{\hbar}\left[\hat{H},\hat{\rho}\right]dt - \frac{1}{2}\mathcal{H}\left[\hat{\Omega}^\dagger\hat{\Omega}\right]\hat{\rho} + \mathcal{J}\left[\hat{\Omega}\right]\hat{\rho}dN. \tag{3.17}$$

Here the evolution due to the Hamiltonian of the system has been added and the rule $dtdN = 0$ has been used. The jump superoperator $\mathcal{J}[\hat{\Omega}]\hat{\rho}$ and the measurement superoperator $\mathcal{H}[\hat{\Omega}^\dagger\hat{\Omega}]\hat{\rho}$ are defined as

$$\mathcal{J}\left[\hat{c}\right]\hat{\rho} \equiv \frac{\hat{c}\hat{\rho}\hat{c}^\dagger}{\langle\hat{c}^\dagger\hat{c}\rangle} - \hat{\rho}, \quad \mathcal{H}\left[\hat{c}\right]\hat{\rho} \equiv \hat{c}\hat{\rho} + \hat{\rho}\hat{c}^\dagger - \left\langle\hat{c}+\hat{c}^\dagger\right\rangle\hat{\rho}, \tag{3.18}$$

respectively. The differential equation (3.17) is called the stochastic master equation (SME). To use this differential equation to solve different event counting problems, the only thing left to do is to derive the operator $\hat{\Omega}$ in a given situation.

In practice the increments dN are realized from the measurement result. Then Eq. (3.17) can be used to simulate the evolution of the quantum state due to the measurement. The Eq. (3.17) is said to give the evolution of the quantum state conditioned on the measurement result. By ignoring the measurement record, or discarding the information given by the measurement, one arrives at the unconditioned master equation. This can be derived[2] by taking the ensemble average of Eq. (3.17). The unconditioned master equation is then

$$d\left\langle\langle\hat{\rho}\rangle\right\rangle = -\frac{i}{\hbar}\left[\hat{H},\left\langle\langle\hat{\rho}\rangle\right\rangle\right]dt + \mathcal{D}\left[\hat{\Omega}\right]\left\langle\langle\hat{\rho}\rangle\right\rangle dt, \tag{3.19}$$

where $\langle\langle\hat{\rho}\rangle\rangle$ is the ensemble averaged density operator and $\mathcal{D}\left[\hat{\Omega}\right]\langle\langle\hat{\rho}\rangle\rangle$ is called the Lindblad superoperator:

$$\mathcal{D}\left[\hat{c}\right]\hat{\rho} \equiv \hat{c}\hat{\rho}\hat{c}^\dagger - \frac{1}{2}\left\{\hat{c}^\dagger\hat{c},\hat{\rho}\right\}. \tag{3.20}$$

3.1.1 Example: Photon detection of a Two Level Atom

An atom coupled to a vacuum field can spontaneously emit a photon to the field. Here the atom is modeled as a two-level system, and its basis is given

[2] More details in Chapter 18.1.1 of Ref. [8]

by the ground state $|g\rangle$ and the excited state $|e\rangle$. The field can be measured with a photon-detector, that clicks when it detects a photon. To study this measurement, Eq. (3.17) can be used. But first we need to figure out what the operator $\hat{\Omega}$ is in this case. The excited atom state decays as

$$\dot{\rho}_{ee} = -\Gamma\rho_{ee} = -\Gamma\left\langle\hat{\sigma}^\dagger\hat{\sigma}\right\rangle, \tag{3.21}$$

where Γ is the spontaneous decay rate and $\hat{\sigma}$ is the atomic two level lowering operator. So Γ tells us the rate at which the photons are emitted to the field. If our detector is perfect and catches every photon, then the rate of decay has to match with the rate of events Eq. (3.7)

$$\left\langle\hat{\Omega}^\dagger\hat{\Omega}\right\rangle = \Gamma\left\langle\hat{\sigma}^\dagger\hat{\sigma}\right\rangle. \tag{3.22}$$

This implies that $\hat{\Omega} = \sqrt{\Gamma}\hat{U}\hat{\sigma}$ with some unitary operator $\hat{U}$. Turns out that choosing $\hat{U} = \hat{I}$ gives the correct results. Then using Eq. (3.17) we see that the dynamics of the atom under continuous detection of its emitted photon is given by

$$d\hat{\rho} = -\frac{i}{\hbar}[\hat{H}_\mathrm{a}, \hat{\rho}]dt - \frac{\Gamma}{2}\mathcal{H}\left[\hat{\sigma}^\dagger\hat{\sigma}\right]\hat{\rho}dt + \mathcal{J}\left[\hat{\sigma}\right]\hat{\rho}dN, \tag{3.23}$$

where $\hat{H}_\mathrm{a} = \hbar\omega\left|e\right\rangle\left\langle e\right|$ is the Hamiltonian for the atom, with the atomic transition frequency ω. The Hamiltonian is chosen so that the ground state has zero energy. An example trajectory of how the measurement affects the photon number $\left\langle\hat{\sigma}^\dagger\hat{\sigma}\right\rangle$ of the atom is presented in Fig. 2. A jump occurs at about $t\Gamma = 2$ and the effect of it is intuitive: when a photon is detected the atom returns to the ground state. We see that the atom seems to be decaying to the ground state even when no photons are detected. The interpretation is that if the atom is excited, then the photon has to be emitted at some point. So the longer it takes for the atom to emit the photon, or for the photon to be detected, the more likely it is to be in the ground state. If we never observe the photon, then the atom had to be in the ground state originally. To see how the atom develops when no photons are detected, we can set $dN = 0$ in Eq. (3.23). We see that there still are additional terms to the Hamiltonian so the measurement affects the evolution even when no photons are detected. This means that the measurement is extracting information from the system at every given moment in time, not just when a photon is detected. [5, 8]

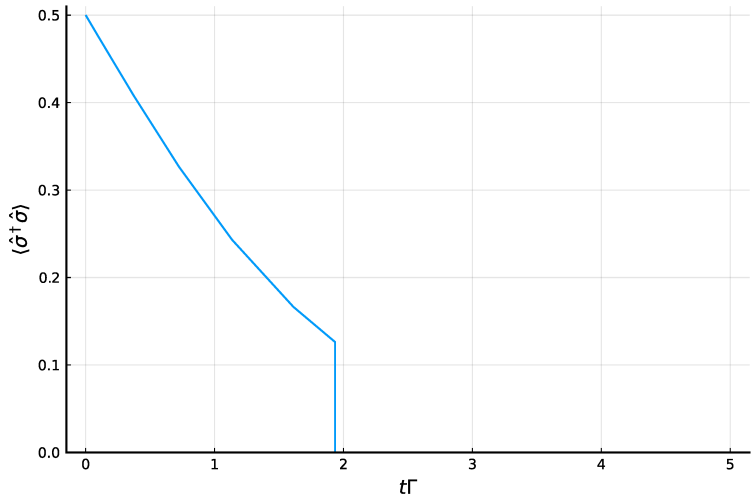

Figure 2: An example trajectory of the effect of the measurement on the photon number. The initial state was $\hat{\rho}_0 = 1/2\left(|0\rangle + |1\rangle\right)\left(\langle 0| + \langle 1|\right)$ and the values used for this plot where $\Gamma = \omega$.

3.2 The Wiener Increment and Itō calculus

For the following chapters we need to discuss a new type of noise, the Wiener noise $W(t)$. The increments of the Wiener noise dW are independent of each other and their probability density is Gaussian

$$P(dW) = \frac{1}{\sqrt{2\pi dt}} e^{-\frac{dW^2}{2dt}}. \tag{3.24}$$

We see that the mean of the Wiener increment is zero and its variance is dt. This type of noise is also referred to as white noise. The variance of the Wiener increment is not an arbitrary choice, it is a consequence of the fact that the infinitesimal increments are Gaussian, independent and identical. Due to these, the Wiener increments must have a variance proportional to dt. The reason, why Gaussian noise is important, is because when one sums over an increasing number of independent random variables the probability density of the sum will tend to a Gaussian. This is know as the central limit theorem. And why this type of noise is important in physical systems, is because the noise in physical systems is often a result of many random events happening at the microscopic level. For example, the total force applied by these events is the sum of each one, and so according to the central limit theorem, the total force will have a Gaussian probability density.

The ordinary rules for solving differential equations, such as $dx^2 = 0$, change

when dealing with the Wiener process. The change in the rules is known as the Itō's lemma: $(dW)^2 = dt$, and the calculus of stochastic differential equations is known as Itō calculus. When dealing with stochastic differential equations with Wiener noise, it is very important to include the second-order terms in dW. Usually the terms that are second-order or higher in the differential dt end up not contributing to the final solution when compared to dt, so that $dt^2 = 0$. Now since the mean of the Wiener increment is zero and since its variance is $\langle (dW)^2 \rangle = dt$, we see[3] that the mean of $(dW)^2$ is comparable to dt, and so the term $(dW)^2$ should not be discarded. The variance of the total contribution of $(dW)^2$ terms can be derived, with the result that it is zero. This means that $(dW)^2$ is actually deterministic and we can use the rule $(dW)^2 = dt$ in calculations. Even though the term $(dW)^2$ is great enough to contribute, terms like $dtdW$ are not, and they can be set to zero in calculations.

To see Itō calculus in action, let us consider that we know the increment of the quantum state $d|\Psi\rangle$ and we want to figure out the increment $d\hat{\rho}$ for the density operator.

$$\begin{aligned}
\hat{\rho}(t) + d\hat{\rho} &= \hat{\rho}(t + dt) && (3.25)\\
&= |\Psi(t + dt)\rangle \langle \Psi(t + dt)| && (3.26)\\
&= (|\Psi(t)\rangle + d|\Psi\rangle)((\langle \Psi(t)| + d\langle \Psi|) && (3.27)\\
&= |\Psi(t)\rangle \langle \Psi(t)| + |\Psi(t)\rangle d\langle \Psi| + d|\Psi\rangle \langle \Psi(t)| + d|\Psi\rangle d\langle \Psi| && (3.28)\\
&\rightarrow d\hat{\rho} = |\Psi(t)\rangle d\langle \Psi| + d|\Psi\rangle \langle \Psi(t)| + d|\Psi\rangle d\langle \Psi|. && (3.29)
\end{aligned}$$

Normally, the term $d|\Psi\rangle d\langle \Psi|$ would vanish, but here it is very important due to the Itō's lemma. For the sake of simplicity, let us consider that $d|\Psi\rangle = \Gamma|\Psi\rangle dt + \sqrt{\Gamma}|\Psi\rangle dW$, for some real constant Γ. Notice that this increment does not conserve the norm, so this example is purely to demonstrate the Itō's lemma. Inserting this to the equation above, we get

$$\begin{aligned}
d\hat{\rho} =& |\Psi\rangle (\Gamma \langle \Psi| dt + \sqrt{\Gamma} \langle \Psi| dW)\\
&+ (\Gamma|\Psi\rangle dt + \sqrt{\Gamma}|\Psi\rangle dW) \langle \Psi|\\
&+ (\Gamma|\Psi\rangle dt + \sqrt{\Gamma}|\Psi\rangle dW)(\Gamma \langle \Psi| dt + \sqrt{\Gamma} \langle \Psi| dW) && (3.30)\\
=& 2\Gamma|\Psi\rangle \langle \Psi| dt + 2\sqrt{\Gamma}|\Psi\rangle \langle \Psi| dW + \Gamma|\Psi\rangle \langle \Psi| dW^2 && (3.31)\\
=& 3\Gamma|\Psi\rangle \langle \Psi| dt + 2\sqrt{\Gamma}|\Psi\rangle \langle \Psi| dW. && (3.32)
\end{aligned}$$

Here the extra $\Gamma|\Psi\rangle \langle \Psi| dt$ term is due to Itō's lemma, and it would not appear in standard calculus. A more detailed explanation for Itō calculus and derivation for the Itō's lemma can be found in Ref. [9].

[3] The expectation value is taken over all of the possible realizations of the noise.

3.3 Homodyne Detection

In the above, the emitted photons were directly measured. Now consider that a local oscillator is added, and the emitted photons from the system of interest are mixed with the photons emitted from the local oscillator by a beam splitter. After this, the mixed field is measured. By local oscillator we mean a monochromatic field i.e. a source of photons of a single frequency. For homodyne detection the frequency of the local oscillator is chosen to be the same as the natural frequency of the system of interest. The homodyne detection measurement scheme is depicted in Fig. 3.

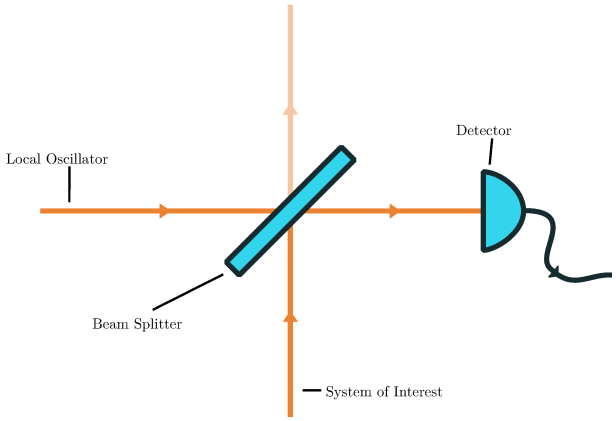

Figure 3: The Measurement scheme for homodyne detection.

Considering the previous example, the mode of the field coupled to the atom can be represented by the operator

$$\hat{C} = \sqrt{\Gamma}\hat{\sigma}, \tag{3.33}$$

and the mode of the local oscillator field by the operator

$$\hat{C}_{\text{loc}} = \sqrt{\Gamma}\hat{a}, \tag{3.34}$$

where $\hat{a}$ is the annihilation operator of the field of the local oscillator. The beam splitter transforms two input modes to two output modes. The output mode on the side of the photodetector is represented by the operator

$$\hat{C}_r = \sqrt{\Gamma}\left(r\hat{\sigma} + \sqrt{1-r^2}\hat{a}\right), \tag{3.35}$$

where r is the field reflection coefficient. The local oscillator can be prepared in the coherent state $|\alpha\rangle$, that is an eigenstate of the lowering operator $\hat{a}$: $\hat{a}\,|\alpha\rangle = \alpha\,|\alpha\rangle$. Using this the above equation is essentially the same as

$$\hat{C}_r = \sqrt{\Gamma}\left(r\hat{\sigma} + \sqrt{1-r^2}\alpha\right). \tag{3.36}$$

Since only one output mode of the beam splitter is being detected, the photons coming from the field of the atom that pass through the beam splitter are wasted. To make sure information is not wasted, the limit $r \to 1$ is taken, meaning that the beam splitter is made as reflecting as possible. If the field reflection coefficient is $r = 1$ we see that this would reduce to simple direct detection of the atom. To circumvent this, the amplitude of the local oscillator field α has to be chosen great enough so that the transmitted field amplitude

$$\beta \equiv \alpha\sqrt{1 - r^2}, \tag{3.37}$$

remains nonzero. Now the field that is being detected changes to

$$\hat{C}_r \to \hat{C}_\beta = \sqrt{\Gamma}\left(\hat{\sigma} + \beta\right). \tag{3.38}$$

One advantage of homodyne detection can now be seen. In the previous example the average detection rate is given by $\langle dN\rangle = \Gamma\left\langle\hat{\sigma}^\dagger\hat{\sigma}\right\rangle dt = \left\langle\hat{C}^\dagger\hat{C}\right\rangle dt$. For homodyne detection the average rate of detection is then

$$\langle dN\rangle = \left\langle\hat{C}_\beta^\dagger\hat{C}_\beta\right\rangle dt = \Gamma\left(\left\langle\hat{\sigma}^\dagger\hat{\sigma}\right\rangle + \left\langle\beta^*\sigma + \beta\hat{\sigma}^\dagger\right\rangle + |\beta|^2\right) dt. \tag{3.39}$$

Now the amplitude of the local oscillator field is chosen to be so great, that the term $\left\langle\hat{\sigma}^\dagger\hat{\sigma}\right\rangle$ can be neglected when compared to $|\beta|^2$. The term $|\beta|^2$ is just a constant term that can be subtracted. The average rate of detection still depends on the state of the atom, since it depends on the term $\left\langle\beta^*\sigma + \beta\hat{\sigma}^\dagger\right\rangle$, but it is essentially boosted by a factor of $|\beta|$. This is advantageous if the detector is prone to unwanted background noise. Another aspect to note is that homodyne detection does not simply measure the photon number of the atom as was in the previous example, it seems to measure something different. What exactly homodyne detection measures will be talked about at the end of this chapter. Before getting into the stochastic master equation for homodyne detection, let us look at the effect of detecting a photon in the homodyne detection scheme has on the state of the atom. The change in the state of the atom is given by

$$\hat{\rho} \to \frac{\hat{C}_\beta\hat{\rho}\hat{C}_\beta^\dagger}{\left\langle\hat{C}_\beta^\dagger\hat{C}_\beta\right\rangle} = \frac{\left(\hat{\sigma} + \beta\right)\hat{\rho}\left(\hat{\sigma}^\dagger + \beta^*\right)}{\langle\left(\hat{\sigma}^\dagger + \beta^*\right)\left(\hat{\sigma} + \beta\right)\rangle}. \tag{3.40}$$

If we consider the atom to be in a pure state $\hat{\rho} = |\Psi\rangle\langle\Psi|$, we see that the effect of the detection on the atom is the projection to a superposition of a photon being detected directly from the atom and the atom being unaffected. This happens since we are unable to distinguish the origin of the photon.

The homodyne detection scheme changed the measurement operator from $\sqrt{\Gamma}\hat{\sigma}$ to $\sqrt{\Gamma}\left(\hat{\sigma} + \beta\right)$. This implies that we can derive the stochastic master equation for homodyne detection by doing the transformation

$$\hat{\sigma} \to \hat{\sigma} + \beta, \tag{3.41}$$

in Eq. (3.23). But if we remove the detector, or discard the information from the measurement, the unconditioned master equation Eq. (3.19), that is

$$d\left\langle\left\langle\hat{\rho}\right\rangle\right\rangle = -\frac{i}{\hbar}\left[\hat{H},\left\langle\left\langle\hat{\rho}\right\rangle\right\rangle\right]dt + \Gamma\mathcal{D}\left[\hat{\sigma}\right]\left\langle\left\langle\hat{\rho}\right\rangle\right\rangle dt, \tag{3.42}$$

in the case of direct detection of the atom, should stay the same. Skipping the short derivation, we see that

$$\mathcal{D}\left[\hat{\sigma}+\beta\right]\hat{\rho} = \mathcal{D}\left[\hat{\sigma}\right]\hat{\rho} - \frac{i}{\hbar}\left[\frac{i\hbar}{2}\left(\beta^*\hat{\sigma} - \beta\hat{\sigma}^\dagger\right),\hat{\rho}\right]. \tag{3.43}$$

Then doing the transformation in Eq. (3.41) and

$$\hat{H} \to \hat{H} - \frac{i\hbar\Gamma}{2}\left(\beta^*\hat{\sigma} - \beta\hat{\sigma}^\dagger\right), \tag{3.44}$$

leaves the unconditioned master equation unchanged. Doing this, a bunch of simplifications[4], and taking the limit of $|\beta| \to \infty$, the stochastic master equation transforms into the form that is called the stochastic master equation for homodyne detection:

$$d\hat{\rho} = -\frac{i}{\hbar}\left[\hat{H},\hat{\rho}\right]dt + \Gamma\mathcal{D}\left[\hat{\sigma}\right]\hat{\rho}dt + \sqrt{\Gamma}\mathcal{H}\left[\hat{\sigma}e^{i\phi}\right]\hat{\rho}dW. \tag{3.45}$$

Here ϕ is the phase of the local oscillator $\beta \equiv |\beta|e^{-i\phi}$. The Wiener increment appears here because of the limit $|\beta| \to \infty$. Due to this limit the counting process $N(t)$ can be approximated as a Gaussian random variable and dN transform as

$$dN \to \Gamma\left\langle\left(\hat{\sigma}^\dagger + \beta^*\right)\left(\hat{\sigma}+\beta\right)\right\rangle dt + \sqrt{\Gamma\left\langle\left(\hat{\sigma}^\dagger+\beta^*\right)\left(\hat{\sigma}+\beta\right)\right\rangle}dW. \tag{3.46}$$

This approximation is valid when the number of events occurred in a time-step is very large, and it follows from the central limit theorem. Since the mean of dW is zero, we see that the mean of the noise term is same as for dN. Previously the noise term could only have values of zero or one, but now the value of the noise in a time-step can be any real number.

To gain understanding of what homodyne detection is actually measuring, we can take a look at the measurement record. The photodetector works by conducting a charge Q for each detected photon. So photon detection causes the current

$$I(t) = Q\frac{dN(t)}{dt}, \tag{3.47}$$

and this current can then be read from the device, providing information about a photon detection event. In homodyne detection the current becomes

$$I(t) = Q\Gamma\left\langle\left(\hat{\sigma}^\dagger+\beta^*\right)\left(\hat{\sigma}+\beta\right)\right\rangle + Q\sqrt{\Gamma\left\langle\left(\hat{\sigma}^\dagger+\beta^*\right)\left(\hat{\sigma}+\beta\right)\right\rangle}\frac{dW(t)}{dt}. \tag{3.48}$$

[4]More details about the derivation can be found in Chapter 18.2 of Ref. [8]

From this the constant current $Q\Gamma|\beta|^2$ can be subtracted and it can then be divided by $Q|\beta|$ so that we get the normalized photocurrent:

$$\begin{aligned}\tilde{I}(t) \equiv & \frac{I(t) - Q\Gamma|\beta|^2}{Q|\beta|} && (3.49)\\ =& \Gamma\left(\frac{\left\langle\hat{\sigma}^\dagger\hat{\sigma}\right\rangle}{|\beta|} + \frac{\left\langle\beta\hat{\sigma}^\dagger + \beta^*\hat{\sigma}\right\rangle}{|\beta|}\right)\\ &+ \sqrt{\Gamma\left(\frac{\langle\hat{\sigma}^\dagger\hat{\sigma}\rangle}{|\beta|^2} + \frac{\langle\beta\hat{\sigma}^\dagger + \beta^*\hat{\sigma}\rangle}{|\beta|^2} + \frac{|\beta|^2}{|\beta|^2}\right)}\frac{dW(t)}{dt} && (3.50)\\ =& \Gamma\left\langle\hat{\sigma}e^{i\phi} + \hat{\sigma}^\dagger e^{-i\phi}\right\rangle + \sqrt{\Gamma}\frac{dW(t)}{dt}, && (3.51)\end{aligned}$$

where the last line follows because of the limit $|\beta| \to \infty$ and because of $\beta/|\beta| = e^{-i\phi}$. Finally we can define the measurement record $dr(t)$ for homodyne detection to be

$$dr(t) \equiv \tilde{I}(t)dt = \Gamma\left\langle\hat{\sigma}e^{i\phi} + \hat{\sigma}^\dagger e^{-i\phi}\right\rangle dt + \sqrt{\Gamma}dW(t). \tag{3.52}$$

Now on average

$$\langle\langle dr(t)\rangle\rangle = \Gamma\left\langle\hat{\sigma}e^{i\phi} + \hat{\sigma}^\dagger e^{-i\phi}\right\rangle dt, \tag{3.53}$$

so we see that homodyne detection extracts information about the quantity $\left\langle\hat{\sigma}e^{i\phi} + \hat{\sigma}^\dagger e^{-i\phi}\right\rangle$. Choosing the phase of the local oscillator to be $\phi = 0$ we get

$$\langle\langle dr(t)\rangle\rangle = \Gamma\left\langle\hat{\sigma} + \hat{\sigma}^\dagger\right\rangle dt = \Gamma\langle\hat{\sigma}_x\rangle dt. \tag{3.54}$$

Similarly if the phase is chosen to be $\phi = \pi/2$ we get

$$\langle\langle dr(t)\rangle\rangle = \Gamma\left\langle i\hat{\sigma} - i\hat{\sigma}^\dagger\right\rangle dt = \Gamma\langle\hat{\sigma}_y\rangle dt. \tag{3.55}$$

Now notice that for a general quantum harmonic oscillator

$$\hat{x} \propto \hat{a}^\dagger + \hat{a}, \quad \hat{p} \propto i\hat{a}^\dagger - i\hat{a}, \tag{3.56}$$

so that the measurement with the phase $\phi = 0$ relates to the measurement of the position of a general quantum harmonic oscillator. Similarly for $\phi = \pi/2$ relates to the measurement of momentum. The quantum harmonic oscillator can be realized with superconducting circuits. The analogues for position and momentum are the flux and charge respectively. Then homodyne detection can be used to measure these quantities. The measurement with $\phi = 0$ is said to measure the $\hat{I}$ quadrature and $\phi = \pi/2$ is said to measure the $\hat{Q}$ quadrature. [5,8]

3.3.1 Example: $\hat{I}$ Quadrature Measurement of a Two Level Atom

In the previous example the photons emitting from the two level atom were directly measured. Now let us see how $\hat{I}$ quadrature measurement, that is homodyne measurement with $\phi = 0$, changes the dynamics. The stochastic differential equation to be solved follows from Eq. (3.45) and is given by

$$d\hat{\rho} = -\frac{i}{\hbar}\left[\hat{H}_a, \hat{\rho}\right]dt + \Gamma\mathcal{D}\left[\hat{\sigma}\right]\hat{\rho}dt + \sqrt{\Gamma}\mathcal{H}\left[\hat{\sigma}\right]\hat{\rho}dW, \tag{3.57}$$

where $\hat{H}_a$ is the Hamiltonian for the atom as in the previous example. An example trajectory can be solved numerically, and how the measurement affects the photon number $\left\langle \hat{\sigma}^\dagger\hat{\sigma} \right\rangle$ and the purity $\mathrm{Tr}\left(\hat{\rho}^2\right)$ is presented in Fig. 6. At large times $t \to \infty$, the effect is similar as in the previous example, the measurement causes the atom to relax to the ground state. But instead of a single discontinuous jump to the ground state, homodyne detection causes noise in every time-step and it can even increase the expectation value of the photon number. This is because the rate of detection depends on the photon number, so that when a lot of photons are detected, we know that the atom was more likely to be excited. [8]

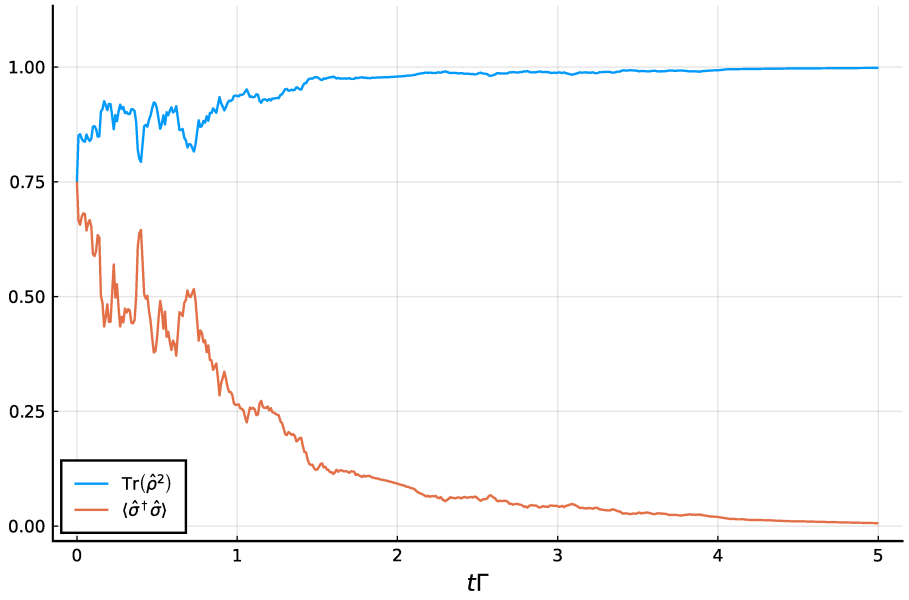

Figure 4: The effect of homodyne detection on the purity and the photon number of the two level atom. The initial state was $\hat{\rho}_0 = 1/2\left|+\right\rangle\left\langle+\right| + 1/2\left|e\right\rangle\left\langle e\right|$, where $\left|+\right\rangle = 1/\sqrt{2}\left(\left|g\right\rangle + \left|e\right\rangle\right)$. The values used where $\phi = 0$ and $\Gamma = \omega$.

3.4 Balanced Homodyne Detection

The same effect of homodyne detection can be achieved with balanced homodyne detection. Instead of measuring only one output mode of the beam splitter, the beam splitter is made equally reflecting and transmitting, and both output modes are measured. Then the photocurrents caused by the detectors are subtracted from each other, and this subtracted signal is then read. The balanced homodyne detection measurement scheme is depicted in Fig. 5.

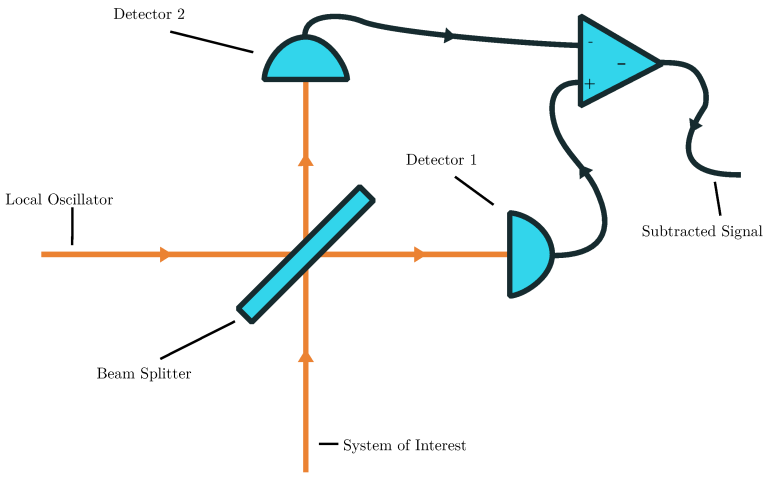

Figure 5: The Measurement scheme for balanced homodyne detection.

To account for the two different detectors detecting the output modes of the beam splitter, we need to introduce two different counting processes: dN_1 and dN_2. If we start from the stochastic master equation for direct detection, Eq. (3.23)

$$d\hat{\rho} = -\frac{i}{\hbar}\left[\hat{H},\hat{\rho}\right]dt - \frac{\Gamma}{2}\mathcal{H}\left[\hat{\sigma}^\dagger\hat{\sigma}\right]\hat{\rho}dt + \mathcal{J}\left[\hat{\sigma}\right]\hat{\rho}dN, \tag{3.58}$$

we can split the counting process dN into two parts $dN = dN_1 + dN_2$, so that the average rate of detection remains the same. These counting processes are defined by the averages

$$\langle\langle dN_1\rangle\rangle = r^2\Gamma\left\langle\hat{\sigma}^\dagger\hat{\sigma}\right\rangle dt, \quad \langle\langle dN_2\rangle\rangle = \left(1-r^2\right)\Gamma\left\langle\hat{\sigma}^\dagger\hat{\sigma}\right\rangle dt, \tag{3.59}$$

where r is the reflection coefficient of the beam splitter. We should also split the other terms in Eq. (3.58) that are related to the measurement. These are

the terms that contain Γ. We end up with

$$\begin{aligned} d\hat{\rho} = &-\frac{i}{\hbar}\left[\hat{H},\hat{\rho}\right]dt \\ &- r^2\frac{\Gamma}{2}\mathcal{H}\left[\hat{\sigma}^\dagger\hat{\sigma}\right]\hat{\rho}dt + \mathcal{J}\left[\hat{\sigma}\right]\hat{\rho}dN_1 \\ &- \left(1-r^2\right)\frac{\Gamma}{2}\mathcal{H}\left[\hat{\sigma}^\dagger\hat{\sigma}\right]\hat{\rho}dt + \mathcal{J}\left[\hat{\sigma}\right]\hat{\rho}dN_2, \end{aligned} \tag{3.60}$$

where the second line represent detector 1 and the third line represents detector 2. Now if we look back to Eq. (3.58) we see that our operators related to the modes of the fields being measured are given by

$$C_{1,\text{direct}} = \sqrt{\Gamma}r\hat{\sigma}, \quad C_{2,\text{direct}} = \sqrt{\Gamma}\sqrt{1-r^2}\hat{\sigma}. \tag{3.61}$$

When we add the local oscillator, the output modes of the beam splitter are given by

$$C_1 = \sqrt{\Gamma}\left(r\hat{\sigma} + \sqrt{1-r^2}\alpha\right), \tag{3.62}$$

for detector 1, and

$$C_2 = \sqrt{\Gamma}\left(\sqrt{1-r^2}\hat{\sigma} - r\alpha\right), \tag{3.63}$$

for detector 2. To add the local oscillator to the Eq. (3.60), we need to do the transformations $C_{1,\text{direct}} \to C_1$ and $C_{2,\text{direct}} \to C_2$. This can be achieved by doing the following transformation

$$\hat{\sigma} \to \hat{\sigma} + \frac{\sqrt{1-r^2}}{r}\alpha, \tag{3.64}$$

for the part relating to detector 1, and

$$\hat{\sigma} \to \hat{\sigma} - \frac{r}{\sqrt{1-r^2}}\alpha, \tag{3.65}$$

for the part relating to detector 2, where α is the amplitude of the local oscillator. Additionally, as before, we would need to transform the Hamiltonian to keep the unconditioned master equation unchanged, but here the effect of these replacements cancels out. Doing these transformations, taking the limit of a strong local oscillator, $|\alpha| \to \infty$, and approximating the counting processes as Gaussian random variables[5] we get the stochastic master equation for balanced homodyne detection:

$$d\hat{\rho} = -\frac{i}{\hbar}\left[\hat{H},\hat{\rho}\right]dt + \Gamma\mathcal{D}\left[\hat{\sigma}\right]\hat{\rho}dt + \sqrt{\Gamma}\mathcal{H}\left[\hat{\sigma}e^{i\phi}\right]\hat{\rho}dW. \tag{3.66}$$

This is the same equation as the stochastic master equation for homodyne detection. The Wiener increment is just given by

$$dW = rdW_1 + \sqrt{1-r^2}dW_2, \tag{3.67}$$

[5]More details about the derivation can be found in Chapter 18.2.6 of Ref. [8]

where dW_1 and dW_2 are the Wiener increments from the approximations for the counting processes dN_1 and dN_2.

Let us again take a look at the measurement record. The photocurrent for detector 1 and detector 2 is given by

$$I_1 = Q_1 \frac{dN_1}{dt}, \quad I_2 = Q_2 \frac{dN_2}{dt}, \tag{3.68}$$

where Q_1 and Q_2 are the charges conducted by the detectors 1 and 2 respectively, for each detection event. We can define the measurement record to be the the difference between the currents I_1 and I_2, so that $dr \equiv (I_1 - I_2)dt$. In the limit of a strong local oscillator we can again approximate the counting process as a Gaussian random variable. If we additionally assume that $Q_1 = Q_2 = Q$ and that the beam splitter is perfectly balanced, $r = 1/\sqrt{2}$, then the measurement record is given by

$$dr \equiv Q\Gamma \left\langle \alpha^* \hat{\sigma} + \alpha \hat{\sigma}^\dagger \right\rangle dt + Q\sqrt{\Gamma}|\alpha| dW, \tag{3.69}$$

where $dW = dW_1/\sqrt{2} + dW_2/\sqrt{2}$. The measurement record for homodyne detection is the same as here, but the measurement record here is lacking normalization. In general the Wiener increment here is not the same as the one in Eq. (3.66). They are the same when the beam splitter is perfectly balanced. We can see that the balanced homodyne detection is an improvement on homodyne detection, since it does not require the beam splitter to be almost completely reflecting and since there is no need to subtract the constant currents from the measurement record. [8]

3.5 Heterodyne Detection

The difference between heterodyne and homodyne detection is in the frequency of the local oscillator. In heterodyne detection the frequency of the local oscillator is not assumed to be the same as the frequency of the system of interest. The frequency difference causes a phase difference that accumulates in time. The phase difference ϕ is given by $\phi = t\Delta$, where $\Delta = \omega_{\text{loc}} - \omega$ is the detuning between the frequencies, and the frequencies ω_{loc} and ω are the frequencies of the local oscillator and the system of interest respectively. Inserting this phase to Eq. (3.45) transforms the equation to the stochastic master equation for heterodyne detection:

$$d\hat{\rho} = -\frac{i}{\hbar}\left[\hat{H}, \hat{\rho}\right] dt + \Gamma \mathcal{D}\left[\hat{\sigma}\right] \hat{\rho} dt + \sqrt{\Gamma} \mathcal{H}\left[\hat{\sigma} e^{it\Delta}\right] \hat{\rho} dW. \tag{3.70}$$

The detuning is assumed to be large, meaning that in every time-step dt there are many cycles in the term $e^{it\Delta}$. The measurement record for heterodyne

detection follows from Eq. (3.52) by replacing the phase

$$dr(t) = \Gamma \left\langle \hat{\sigma} e^{it\Delta} + \hat{\sigma}^\dagger e^{-it\Delta} \right\rangle dt + \sqrt{\Gamma} dW(t). \tag{3.71}$$

The measurement record oscillates, but these oscillations can be removed by multiplying the equation above with the function $e^{-t\Delta}$. This gives

$$\Gamma \left\langle \hat{\sigma} + \hat{\sigma}^\dagger e^{-2it\Delta} \right\rangle dt + \sqrt{\Gamma} e^{-it\Delta} dW(t) \approx \Gamma \langle \hat{\sigma} \rangle \, dt + \sqrt{\Gamma} dV(t), \tag{3.72}$$

where $dV \equiv e^{-it\Delta} dW$ is called the frequency-shifted noise process. The approximation is valid because the term $\hat{\sigma}^\dagger e^{-2it\Delta}$ oscillates rapidly, and thus vanishes when averaged over any reasonable time. From the measurement record we see that heterodyne detection extracts information about the quantity $\langle \hat{\sigma} \rangle$, so that it extracts information about both of the quantities $\langle \hat{\sigma}_x \rangle$ and $\langle \hat{\sigma}_y \rangle$. An intuitive, but not rigorous, explanation for this is given in Fig. 6. [8]

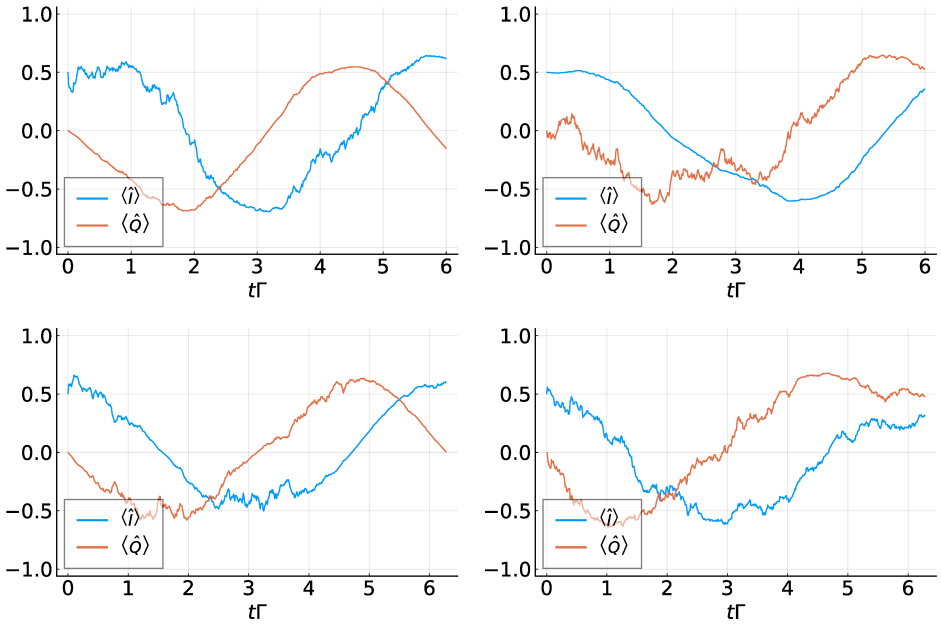

Figure 6: On top left is the $\hat{I}$ quadrature homodyne measurement, and on the top right is the $\hat{Q}$ homodyne quadrature measurement. The two plots on the bottom are of heterodyne measurement, with a smaller and a larger phase difference Δ. The equation solved in these is Eq. (3.45) with $\Gamma = \omega/10$, and $\phi = 0$ and $\phi = \pi/2$ respectively. The Hamiltonian here is not particularly relevant, and was chosen to be $\hat{H} = \omega\hat{a}^\dagger\hat{a}$. The same Hamiltonian was used in all of the four plots. We see that when measuring the $\hat{I}$ quadrature, the changes in the value of $\left\langle \hat{Q} \right\rangle$ are smoother when compared to the values of $\left\langle \hat{I} \right\rangle$. Similar thing can be seen in the plot on the top right, with the conclusion we can see what is being measured from the jaggedness of the plots. In heterodyne detection the frequency difference causes the phase to change, which causes the measurement to alternate between $\hat{I}$ quadrature measurement and $\hat{Q}$ quadrature measurement. This can be seen in the figure on bottom left, where the frequency difference is small. The equation solved in the bottom two pictures is Eq. (3.70), where $10\Gamma = \omega = \Delta$ on bottom left and $10\Gamma = \omega = 100\Delta$ on bottom right. When the change in the value of $\left\langle \hat{Q} \right\rangle$ is jagged, the change in the value of $\left\langle \hat{I} \right\rangle$ is smooth and this seems to alternate as time goes on, meaning that on bottom left the measurement seems to alternate between the two kinds of measurements. When the phase difference is large, heterodyne detection effectively measures both of the quadratures in the same time step. This is seen on the graph on bottom right, where the change in both of the curves is jagged. The initial state in all of these was $\hat{\rho}_0 = 1/4\left(|0\rangle + |1\rangle\right)\left(\langle 0| + \langle 1|\right) + 1/4\,|0\rangle\langle 0| + 1/4\,|1\rangle\langle 1|$, so that the state is mixed.

4 The Transmon Device and the Bose-Hubbard Model

Quantum computers require quantum bits, or qubits, to operate. One way to realize a qubit is with superconducting circuits [10]. The goal of this chapter is to introduce the transmon device [11], a superconducting circuit element that can be operated as a qubit. For example the IBM quantum computer uses transmons as its qubits [12]. To understand the transmon device, some basics of superconductivity are needed, and these are briefly introduced next. For the following chapters we will need to know how to model several transmons connected to each other as a chain, and for this the Bose-Hubbard model [13] is introduced.

4.1 Superconductivity and the Josephson Junction

Some metals become superconductors when cooled sufficiently. This can be seen e.g. in the resistance of the metal, which vanishes once the metal becomes superconducting. In superconductors the electrons become bound to each other and form pairs. These pairs are formed between electrons with the opposite momentum and spin, and they are called Cooper pairs. Since the Cooper pairs consist of two electors with opposite spin they are bosons, capable of occupying the same quantum state. In an ideal superconductor all of the Cooper pairs are condensed into the same ground state, and the whole superconductor is described by a single macroscopic quantum state. Breaking apart the Cooper pairs requires energy. This causes an energy gap between the ground state and the excited states. Superconductors operate at very low temperatures so that the superconductor is in its ground state and it does not have any energy to release to the environment, while the environment does not have enough energy to overcome the energy gap. Because of these properties, superconductors are resistant to decoherence and dissipation caused by the environment. [5, 10, 14]

The Josephson junction is a circuit element which is formed by two superconductors separated with an insulative gap. Since the superconductors obey quantum mechanics, the Cooper pairs are capable of tunneling through the insulator resulting in a supercurrent between the superconductors. Josephson junctions also inherently have capacitance. The Hamiltonian that describes an isolated Josephson junction is given by

$$\hat{H} = 4E_{\mathrm{C}}\hat{n}^2 - E_{\mathrm{J}}\cos\hat{\phi}, \tag{4.1}$$

where $\hat{n}$ relates to the number of Cooper pairs on one of the superconductors and $\hat{\phi}$ relates to the phase difference between the superconductors. The first term describes the energy associated with charging the junction with Cooper

pairs where $E_{\mathrm{C}} = e^2/2C$ is the charging energy of a single electron and C is the capacitance of the junction. The second term describes the energy regarding the inductance of the junction. E_{J} is the Josephson energy which gives the energy associated with the tunneling of the Cooper pairs. [15]

4.2 The Transmon Device

By capacitively coupling the Josephson junction to a voltage source, a qubit can be made. This type of a qubit is called a Cooper pair box qubit [14]. The voltage source causes an offset charge n_g so that the Hamiltonian for the Cooper pair box is

$$\hat{H} = 4E_{\mathrm{C}} \left(\hat{n} - n_g\right)^2 - E_{\mathrm{J}} \cos\hat{\phi}. \tag{4.2}$$

Due to the gate capacitance C_g introduced with the voltage source the charging energy is now $E_{\mathrm{C}} = e^2/2(C_{\mathrm{J}} + C_g)$. The circuit diagram for this is depicted in Fig. 7 on the left. The first three energy levels are shown in (a) in Fig. 8. We see that the energy levels are not evenly separated unlike it would be for a harmonic oscillator. This is called anharmonicity. We also see that the Cooper pair box is sensitive to noise in n_g. This noise changes the transition energy from one state to another which then would affect the operating frequency of the Cooper pair qubit. As seen in the figure, the sensitivity to noise in n_g can be improved by operating the qubit at a higher ratio of $E_{\mathrm{J}}/E_{\mathrm{C}}$. By introducing a new capacitor C_B parallel to the Josephson junction the ratio can be controlled. Including this capacitor the charging energy becomes $E_{\mathrm{C}} = e^2/2(C_{\mathrm{J}} + C_g + C_B)$, and higher values of the ratio $E_{\mathrm{J}}/E_{\mathrm{C}}$ are now achievable. This is called the transmon device and the circuit diagram for it can be seen in Fig. 7 on the right. Increasing the ratio also decreases the anharmonicity which is crucial for the different energy levels to be distinguishable and for the transmon to be usable as a qubit. Luckily for the transmon the anharmonicity decreases slower than the susceptibility to the noise in n_g, so that there exists a sweet spot where the reduction to susceptibility to noise is significant but the transmon is still operable as a qubit. Together these lead to significant improvement on the dephasing time when compared to the Cooper pair box qubit. The transmon uses two Josephson junctions in parallel instead of just one. Two Josephson junctions in parallel is called a SQUID (superconducting quantum interference device) and it enables the Josephson energy E_{J} to be controlled by an external magnetic flux. The Hamiltonian for a single transmon is the same as in Eq. (4.2), but where E_{C} and E_{J} have been changed as mentioned before. But the form of the transmon Hamiltonian that we need is

$$\hat{H} = \left(\sqrt{8E_{\mathrm{J}}E_{\mathrm{C}}} - E_{\mathrm{C}}\right)\hat{n} - \frac{E_{\mathrm{C}}}{2}\hat{n}\left(\hat{n} - 1\right) \equiv \hbar\omega\hat{n} - \frac{\hbar U}{2}\hat{n}\left(\hat{n} - 1\right), \tag{4.3}$$

which is derived from Eq. (4.2) by taking the second order Taylor expansion of the cosine term, approximating the resulting Hamiltonian of an anharmonic oscillator to the first order with the perturbation theory, reordering term through the commutation relation of the annihilation and the creation operator and by neglecting constants. A realization of the transmon device is depicted in Fig. 9 together with the SQUID and a Josephson junction. [11]

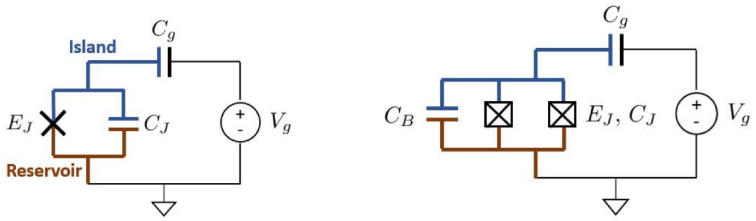

Figure 7: Circuit diagram for the Cooper pair box on the left, and that for the transmon on the right. The Josephson junction with the capacitance C_{J} is depicted by a cross inside of a box. Two of these are connected in parallel to an additional capacitance C_B forming the transmon device. The picture is taken from [15]

.

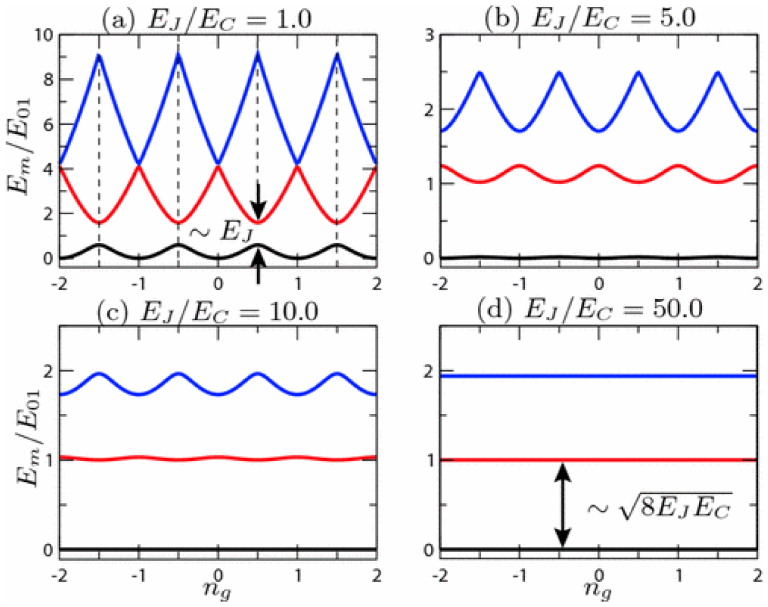

Figure 8: The first three energy levels of the Hamiltonian (4.2) as a function of the offset charge n_g. The energies are given in the units of the transition energy $E_{01} = E_1 - E_0$ evaluated at $n_g = 1/2$. This shows simultaneously the transformation from the Cooper pair box to the transmon, and the cost in anharmonicity for the reduction in susceptibility to the noise in n_g, as the ratio $E_\mathrm{J}/E_\mathrm{C}$ is increased. The picture is taken from [11].

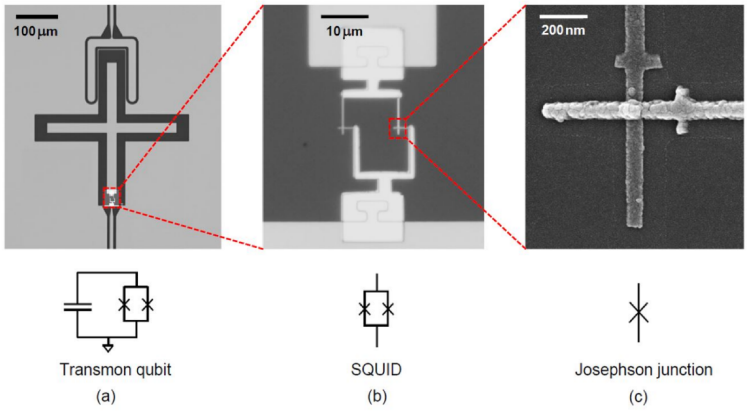

Figure 9: The realization of the transmon device (a), together with the SQUID (b) and the Josephson junction (c). The capacitance C_B of the transmon is achieved with the cross shape seen in (a). The picture is taken from [15].

4.3 The Bose-Hubbard Model and the Transmon Chain

When several transmons are placed near each other, they can interact so that excitations can hop from one transmon to another. The dynamics of such a system is captured by the Bose-Hubbard model, the boson variant of the Hubbard model. In general the Bose-Hubbard model describes a lattice where bosons are stored on sites, the sites can interact with their neighbouring sites so that the bosons can hop from one site to another, and where the bosons on-site can interact among themselves. By introducing multiple transmons to Eq. (4.3) and allowing them to interact, we arrive at the Bose-Hubbard Hamiltonian, which is given by

$$\hat{H}_{\mathrm{BH}}/\hbar = \omega \sum_i \hat{n}_i - \frac{U}{2} \sum_i \hat{n}_i \left(\hat{n}_i - 1\right) + J \sum_i^{N-1} \left(\hat{a}_i^\dagger \hat{a}_{i+1} + \hat{a}_{i+1}^\dagger \hat{a}_i\right). \quad (4.4)$$

Here $\hat{a}_i$ is the bosonic annihilation operator of site i and $\hat{n}_i$ is the number operator for that site. The transition frequency of the ground state and the first excited state is given by ω which also describes the chemical potential of the bosons. The anharmonicity U describes the interactions of the bosons on-site. The interaction can be repulsive $(U < 0)$ or attractive $(U > 0)$. The last term describes the interaction between the transmons, that is the hopping of bosons from one site to another where J gives the hopping rate. Four transmon qubits are depicted in Fig. 10. [13, 16]

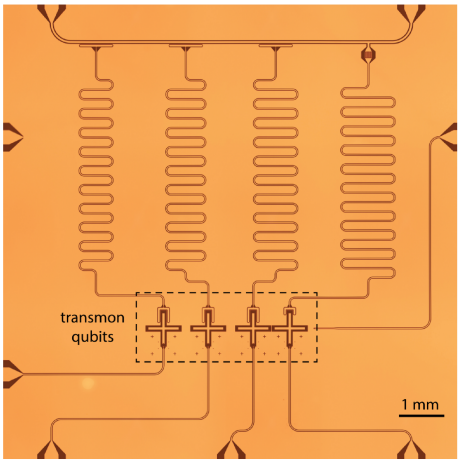

Figure 10: Four transmons together with the microwave network needed to measure and control the state of the transmons. On the top are the readout resonators which can be used to measure the state of the transmon. The same lines can also be used to control the state of the transmon by sending microwave pulses at the transmon transition frequency instead of the resonator frequency [17]. On the bottom there are the flux bias lines used to change to transition frequency of the transmon. The picture is taken from [15].

5 Heterodyne Detection of a System of Transmons

For transmons to be useful they need to be controllable and measurable. This chapter introduces the superconducting cavity [5] and its role in the control and measurement of the transmons. Some examples on how to use microwave pulses to control [17] the state of qubits are presented, followed by an introduction to phase-preserving amplification [5, 18], necessary for realizing continuous measurements. Finally this chapter provides a realistic stochastic master equation [19] for the heterodyne detection of transmons. Four transmons together with the required architecture to measure and control them is depicted in Fig. 10.

5.1 Superconducting Cavity

A stripline of superconducting material can support several different modes of the electromagnetic field, similarly to an optical cavity. This type of a strip is therefore referred to as a superconducting cavity. When the strip is made longer, the superconducting line effectively supports a continuum of traveling waves. These type of lines are called transmission lines. The transmission line can be coupled capacitively to the cavity, enabling signals to be sent into the cavity and the measurement of signals coming from the cavity. The transmission line cavity setup is analogous to an optical cavity coupled to the outside world. A qubit can be coupled to the cavity by simply inserting it inside the cavity. A coplanar wave-guide is depicted in Fig. 11 which realizes the superconducting cavity. [5]

The dynamics of a qubit interacting with a single mode of the superconducting cavity is described by the Jaynes-Cummings Hamiltonian

$$\hat{H}_{\mathrm{JC}} = \hbar\omega\left(\hat{a}^\dagger\hat{a} + \frac{1}{2}\right) + \hbar\frac{\Omega}{2}\hat{\sigma}_z + \hbar g\left(\hat{a}^\dagger\hat{\sigma}^- + \hat{a}\hat{\sigma}^+\right), \tag{5.1}$$

where the first term describes the superconducting cavity, the second term describes the qubit and the last term describes the interaction between the qubit and the cavity with $\hat{\sigma}^-$ and $\hat{\sigma^+}$ being the lowering and rising operators of the qubit. Coupling of the qubit to other modes of the superconducting cavity causes decay of the excited qubit state. The cavity couples to the transmission lines which causes decay of the cavity. These can be modelled with additional terms in the Hamiltonian Eq. (5.1), but they have been omitted here. When there is a large detuning between the cavity resonance frequency ω and the qubit transition frequency Ω compared to the coupling g i.e. $\Delta = \Omega - \omega \gg g$, the cavity qubit system is said to be in the dispersive regime. In the dispersive

regime the Jaynes-Cummings Hamiltonian can be approximated as

$$\hat{H}_{\mathrm{JC}} \approx \hbar \left(\omega + \frac{g^2}{\Delta} \hat{\sigma}_z \right) \hat{a}^\dagger \hat{a} + \frac{\hbar}{2} \left(\Omega + \frac{g^2}{\Delta} \right) \hat{\sigma}_z. \tag{5.2}$$

The important part here is in the first parenthesis. We see that the state of the qubit changes the cavity transition frequency by $\pm g^2/\Delta$. This enables the measurement of the qubit state by probing the cavity with microwave pulses. Additionally in Eq. (5.2) we see that the qubit transition frequency is Lamb shifted by g^2/Δ. [20]

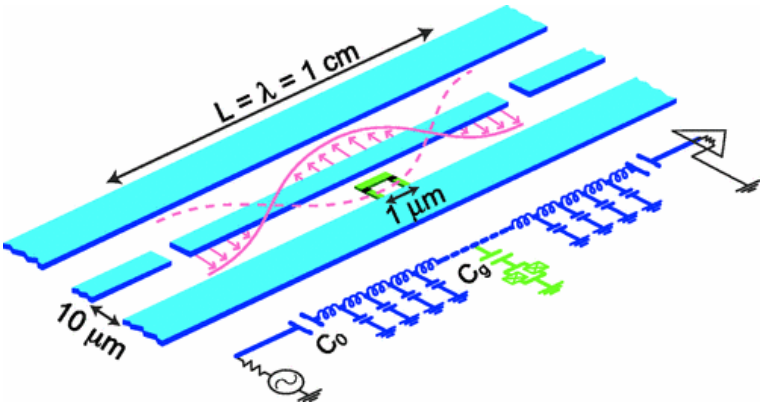

Figure 11: The coplanar wave guide consists of a superconducting stripline between the ground planes forming the cavity [21]. On the left and the right you can see short segments of the input and the output transmission lines, and between them is the cavity together with a Cooper pair box qubit, capacitively coupled to the cavity. The picture is taken from [20].

5.2 Controlling a Transmon Qubit

For realizing quantum computation, quantum gates are needed. Quantum gates change the state of qubits, and can be described as unitary operators. Quantum gates can operate on any number of qubits. Quantum gates that operate on one qubit can be represented as rotation around the Bloch sphere. An example of a multi-qubit gate is the controlled NOT (CNOT) gate which switches the state of a target qubit based on the state of a control qubit. It turns out that any unitary operation on any number of qubits can be realized by using only single qubit gates together with CNOT gates. This set of gates is said to be universal, meaning that any quantum computation can be realized just by using these gates. Note that there exists other sets that are universal, and not every kind of a single qubit gate is needed for universality. [22]

Quantum gates can be realized by coupling a qubit to a superconducting cavity and by using transmission lines to drive the cavity. By driving the cavity with specific microwave pulses the qubit can be rotated around any axis of the Bloch sphere, realizing a single qubit quantum gate. The driven cavity qubit system is described by the Jaynes-Cummings Hamiltonian Eq. (5.1) with an additional $\hat{H}_{\mathrm{D}}$ term describing the drive. In the dispersive regime ($\Delta = \Omega - \omega \gg g$) and when the cavity is driven near the qubit transition frequency, the Hamiltonian is effectively given by

$$\hat{H} \approx \Delta_\omega \hat{a}^\dagger \hat{a} + \frac{\Delta_\Omega}{2}\hat{\sigma}_z + \frac{\Omega_R}{2}\hat{\sigma}_x, \tag{5.3}$$

where $\Delta_\omega = \omega - \omega_d$ is the detuning of the cavity and the drive frequency ω_d, $\Delta_\Omega = \Omega + g^2/\Delta - \omega_d$ is the detuning between the Lamb shifted qubit and the drive and Ω_R is the Rabi frequency. We see that by choosing $\Delta_\Omega = 0$ we get rotation around the x-axis, realizing what is called a bit-flip gate. By controlling Δ_Ω, Ω_R and the phase of the drive, rotation around any axis on the Bloch sphere can be achieved, realizing any single qubit gate.

A gate known as the $\sqrt{\mathrm{iSWAP}}$ gate is known to be universal together with single qubit gates. This gate can be realized by simply inserting two qubits inside the same superconducting cavity and greatly detuning them from the cavity. In this situation the qubits do not effectively couple to the cavity, but interact through it with one another producing a term that realizes the $\sqrt{\mathrm{iSWAP}}$ gate, when the qubits are allowed to interact for a certain period. To achieve this we need to be able to turn on and off the gate at will. This can be achieved by controlling the tuning between the qubits. Tuning the qubits off-resonance with one another turns off the interaction. The interaction can be turned back on by tuning the qubits to be on-resonance. One way to tune the transition frequency of transmons qubits is with flux bias lines. [17]

5.3 Phase-Preserving Linear Amplifier

A measurement produces a classical number that describes the value of the measured observable. For the measurement to be sensible the uncertainty of the measurement result has to be as minimal as possible. To achieve this, real measurements require amplification of the measurement signal so that the signal being measured can be reliably recorded over background noise. It is crucial for the amplifiers to introduce as little noise as possible. Measurement of noisy signals is inefficient, meaning that some of the information in the signal is lost among the noise. So to achieve efficient measurement amplifiers that add as little as noise as possible are required. Continuous measurement is analogous to an amplification process that produces a classical signal. [5]

The signal we want to amplify is carried by a single-mode field [23]

$$\hat{S}(t) = \frac{1}{2}\left(\hat{a}e^{-i\omega t} + \hat{a}^{\dagger}e^{-i\omega t}\right) = \frac{1}{\sqrt{2}}\left(\hat{I}\cos\omega t + \hat{Q}\sin\omega t\right), \tag{5.4}$$

where $\hat{I}$ and $\hat{Q}$ are the amplitude and the phase quadrature of the mode, with the relation $\hat{a} = 1/\sqrt{2}\left(\hat{I} + i\hat{Q}\right)$. There are two types of linear amplifiers [24]. Phase-preserving linear amplifiers amplify both of the quadratures but the noise they add is quantum limited, meaning that phase-preserving linear amplifiers always add some noise to the output signal. Phase-sensitive linear amplifiers amplify one of the quadratures while weakening the other. These type of amplifiers do not need to add any noise [18] by producing a squeezed state, where the noise in one quadrature is reduced at the expense of more noise in the other. Since in heterodyne measurement we are interested in both of the quadratures, phase-preserving linear amplifiers are preferred.

In a simple picture, a phase-preserving linear amplifier takes in an input mode described by the operator $\hat{a}_{\mathrm{in}}$ and produces an output mode $\hat{a}_{\mathrm{out}}$. The relation between these two is given by

$$\hat{a}_{\mathrm{out}} = \sqrt{G}\hat{a}_{\mathrm{in}} + \hat{N}, \tag{5.5}$$

where G is the gain of the amplifier and the operator $\hat{N}$ describes the noise added by the amplifier. The operator $\hat{N}$ is necessary so that the commutation relations of the output mode are preserved. It can be shown that the noise added by the amplifier has a minimum. In the high gain limit this is given by

$$\frac{\left(\Delta\hat{a}_{\mathrm{out}}\right)^2}{G} \geq \left(\Delta\hat{a}_{\mathrm{in}}\right)^2 + \frac{1}{2}, \tag{5.6}$$

where $\left(\Delta\hat{a}_{\mathrm{in}}\right)^2$ is the noise in the input signal and $\left(\Delta\hat{a}_{\mathrm{out}}\right)^2$ is the noise in the output signal. Eq. (5.6) says that in the high gain limit a phase-preserving linear amplifier is forced to add noise to the signal, which is equal to there being an extra half a quantum of noise in the input signal. In more detail, a phase-preserving linear amplifier achieves amplification by taking advantage of an extra mode. This extra mode is referred to as the idler mode, and it is the source of the extra noise in the amplification. The quantum limit Eq. (5.6) originates from the zero-point fluctuations of the idler mode. [18]

A phase-preserving linear amplifier can be realized with a Josephson parametric converter [24]. Simplified, it consists of four Josephson junctions placed in a ring, some capacitors and two resonators (resonator A and resonator B). The resonator A couples to the signal mode and the resonator B couples to the idler mode. Additionally a pump mode is required which provides the energy required for the amplification. When the pump mode is driven at the frequency that is the

sum of the signal mode and the idler mode the Josephson parametric converter functions as a phase-preserving linear amplifier. Additionally when the resonator A is in resonance with the signal mode and when the resonator B is in resonance with the idler mode, and in the limit of a wide amplification bandwidth, the input-output relations for the signal and the idler mode are essentially given by

$$\hat{a}_{\text{si, out}} = \sqrt{G}\hat{a}_{\text{si, in}} + \sqrt{G-1}\hat{a}^{\dagger}_{\text{id, in}}, \tag{5.7}$$

$$\hat{a}_{\text{id, out}} = \sqrt{G}\hat{a}_{\text{id, in}} + \sqrt{G-1}\hat{a}^{\dagger}_{\text{si, in}}. \tag{5.8}$$

The Josephson parametric converter as an amplifier is capable of achieving power gain of at least 40 dB and the upper bound on the noise added by the amplifier is three times the quantum limit. [19, 24]

5.4 Heterodyne Detection of Transmons

We now have all the tools required for a realistic continuous measurement of transmons. The measurement of a transmon has been achieved in practise in Ref. [25], but here the discussion follows Ref. [19]. The transmons that we want to measure are dispersively coupled to separate superconducting cavities. The cavities are driven through their input ports. The state of the cavities develop to a coherent state whose properties are dependant on the state of the transmon, enabled by the dispersive coupling. The different coherent states can be differentiated by their $\hat{I}$ and $\hat{Q}$ quadrature values. The cavities are connected through their output ports with transmission lines to amplifiers. The $\hat{I}$ and $\hat{Q}$ quadrature of the signal leaving the amplifier are then detectable, realizing heterodyne measurement. The stochastic master equation describing the heterodyne detection of transmons is given by

$$\begin{aligned} d\hat{\rho} = &-\frac{i}{\hbar}\left[\hat{H}_{\text{BH}}, \hat{\rho}\right] + \sum_i \frac{\Gamma^i}{2}\mathcal{D}\left[\hat{\sigma}^i\right]\hat{\rho}dt \\ &+ \frac{\sqrt{\Gamma^i}}{2}\mathcal{H}\left[\hat{\sigma}^i\right]\hat{\rho}dW_I^i + \frac{\sqrt{\Gamma^i}}{2}\mathcal{H}\left[i\hat{\sigma}^i\right]\hat{\rho}dW_Q^i, \end{aligned} \tag{5.9}$$

where Γ^i is the measurement rate for the i-th transmon, $\hat{\sigma}^i$ is the measurement operator and dW_I^i and dW_Q^i are the Wiener increments for the measurement of the $\hat{I}$ and $\hat{Q}$ quadrature. In the high gain limit the amplification process followed by the heterodyne detection of the signal is analogous to a 50-50 beam splitter followed by phase-sensitive amplification and detection of both of the output modes of the beam splitter, resulting in two different noise processes. In a numerical problem the number of elements in the density matrix $\hat{\rho}$ is given by $d = (s^n)^2$, where s is the dimensions of a single transmon and n is the number of transmons. In numerics the transmon can not have infinite basis states so the

state space of the transmon has to be cut, defining the value of s. The size of the density matrix $\hat{\rho}$ quickly grows as more transmons are introduced, causing the numerical problem to require more memory and in general become slower to solve. To achieve larger systems we can use the stochastic Schrödinger equation version of Eq. (5.9), which is given by

$$\begin{aligned} d\left|\Psi\right\rangle = &-\frac{i}{\hbar}\hat{H}_{\mathrm{BH}}\left|\Psi\right\rangle - \frac{\Gamma}{4}\hat{\sigma}^2\left|\Psi\right\rangle dt + \frac{\Gamma}{4}\left\langle\hat{\sigma}\right\rangle\hat{\sigma}\left|\Psi\right\rangle dt - \frac{\Gamma}{8}\left\langle\hat{\sigma}\right\rangle^2\left|\Psi\right\rangle dt \\ &+ \frac{\sqrt{\Gamma}}{2}\left(\hat{\sigma} - \left\langle\hat{\sigma}\right\rangle\right)\left|\Psi\right\rangle dW_I - \frac{\sqrt{\Gamma}}{2}i\hat{\sigma}\left|\Psi\right\rangle dW_Q, \end{aligned} \tag{5.10}$$

where only one transmon is being measured. The number of elements required to represent the state vector is $\sqrt{d} = s^n$. The connection between the stochastic master equation and the stochastic Schrödinger equation is [8]

$$d\hat{\rho} = \left(d\left|\Psi\right\rangle\right)\left\langle\Psi\right| + \left|\Psi\right\rangle\left(d\left\langle\Psi\right|\right) + \left(d\left|\Psi\right\rangle\right)\left(d\left\langle\Psi\right|\right), \tag{5.11}$$

where the last term does not vanish since in Itō calculus we have that $\left(dW_I\right)^2 = \left(dW_Q\right)^2 = dt$. In the following chapters both of these equations will be solved and studied numerically.

6 Simulating Continuous Measurement With Julia

This chapter introduces the programming language Julia, and explains how it can be used together with the differential equations package to solve the continuous measurement equations. Solving stochastic differential equations numerically with the differential equations package is demonstrated with examples. These examples focus on stochastic differential equations with jumps and equations with Wiener noise. Optimizing performance in Julia is shortly introduced, followed by the chapters presenting the most relevant parts of the code that was used to solve the quantum mechanics specific stochastic differential equation problems.

6.1 Julia as a Programming Language

One of the design principles of Julia [26] was to create a language that combines some of the best features of various different programming languages, to achieve code that is easy to write and very fast [27]. Julia is not an object-oriented language, and writing code in Julia feels similar to writing code in Python. Similar to Python, Julia is a dynamic language, meaning that defining the type of the variables is not necessary, unlike in languages like C. Julia takes advantage of multiple dispatch, so that in Julia it is possible to define the same function to do different tasks depending on the arguments of the function. Julia uses this to achieve type-specific code. Another key functionality of Julia is that Julia requires the code to be compiled to machine code before running. Languages like C and C++ are similar to Julia in this aspect. Julia achieves performance that rivals C by translating a given function to several different type-specific methods, which are then compiled and ran [28]. The performance of Julia has been compared to other programming languages in Fig. 12.

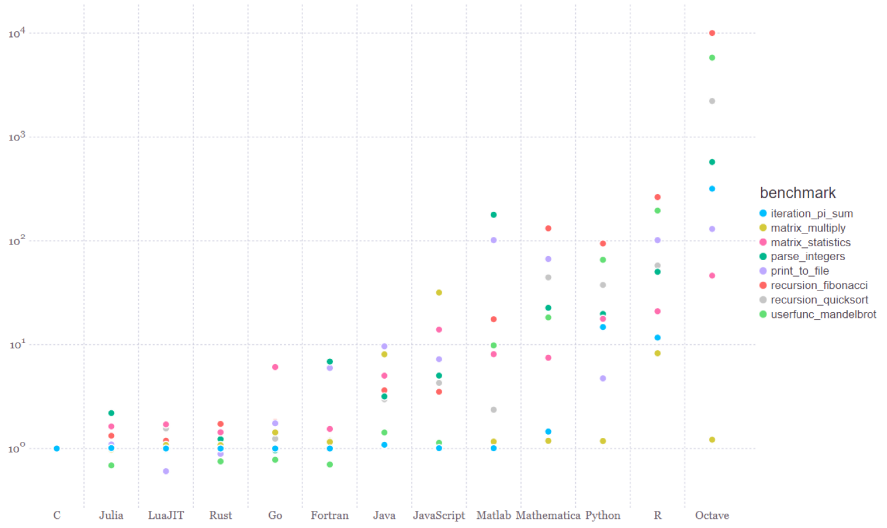

Figure 12: A comparison of performance time between different programming languages for common code patterns and algorithms. The performance times are normalized against the C implementation times. This figure should be taken as a general indication of Julia's performance. The picture is taken from [29].

6.2 Solving Stochastic Differential Equations With the Differential Equations Package

The differential equations package [30] provides various well optimized tools for solving different kinds of differential equations. We can use it to numerically solve the stochastic master equations for quantum jumps Eq. (3.17), homodyne detection Eq. (3.45) and heterodyne detection Eq. (3.70), and additionally the stochastic equations in particular to the measurement of transmons, equations (5.9) and (5.10). This Chapter provides examples on how the package can be used to solve the jump problem and stochastic differential equations with Wiener noise.

6.2.1 Solving the Jump Problem

Consider the following stochastic differential equation

$$dx = f dt + g dN, \tag{6.1}$$

where $x \in \mathbb{R}$, and where f and g are some general functions of arbitrary arguments, that denote the deterministic part and the stochastic part respectively.

In the stochastic part, the dN is the increment of the counting process $N(t)$, which was used in Chapter 3.1. In the differential equations package these type of problems are known as jump problems. To solve this, we need to write a function in code that describes f, write a function that describes the effect of g and define the rate of the events. For a more concrete example, consider that

$$x(0) = 1, \quad f = x, \quad g = -\frac{1}{2}x, \quad \lambda = t, \tag{6.2}$$

so that $x(t)$ is an exponentially rising function except when it is interrupted by jumps which then halve the value of it. The rate of events λ increases linearly with time so that eventually the value of x starts to approach zero, since the rate of events is so high. The function f can be defined in Julia as

```
function f(dx, x, p, t)
    dx[1] = x[1]
end
```

Notice here that due to syntax, the x in the code is expected to be a vector even though for us it is a real number, thus requiring the square brackets. Here `p` is a parameters argument that can be used to store all the relevant parameters that are needed for the differential equations, but here it is required only for syntax reasons. The effect of the function g can be defined as

```
function affect!(integrator)
    integrator.u.u[1] *= 0.5
end
```

Here the `integrator.u.u` is the same as `x` in the previous function. The rate can be defined similarly as

```
function rate(x, p, t)
    return t
end
```

Note that since these functions in code are simple, they could be written on one-line, e.g. `rate(x, p, t) = t`. In Julia by default functions return the value on the last line, so the `return` keyword is not necessary, but it has been written here for clarity. Now that the functions defined, we need to define the problem accordingly to the syntax of the differential equations package.

```
x_0 = [1.0]
tspan = (0.0, 6.0)
jump = VariableRateJump(rate, affect!)

problem = ODEProblem(f, x_0, tspan)
jumpProblem = JumpProblem(problem, Direct(), jump)
solution = solve(jumpProblem, Tsit5())
```

We first define the initial value of `x`, the time for which we want to solve the time evolution and we define the jump. Specifically for `VarialbeRateJumps` one needs to use `integrator.u.u` in the `affect!` function to get the value of `x`. For `VariableRateJumps` `integrator.u` is the type of `ExtentedJumpArray` which is not the same as `x`. After this an `ODEProblem` is defined, which is used together with the `jump` to define the `JumpProblem`. Finally, the `jumpProblem` can be solved, and the solution can be plotted. In the `JumpProblem` function the function `Direct` refers to stochastic simulation algorithm. In the `solve` function the function `Tsit5` refers to the algorithm used to solve the differential equation. The solution to this has been plotted in Fig. 13.

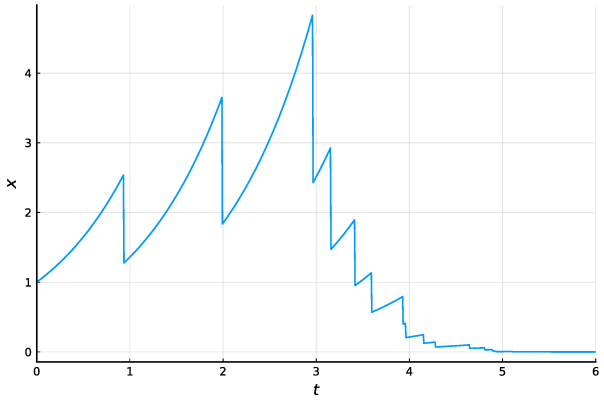

Figure 13: A numerically solved trajectory of Eq. (6.1). The value of x has been plotted as a function of time. We see that x begins to approach zero, since the rate of jumps is getting higher and higher.

6.2.2 Solving Equations With Wiener Noise

Let $x \in \mathbb{R}$ as before, together with the stochastic differential equation

$$dx = f dt + \sum_i g_i dW_i, \tag{6.3}$$

where f and g_i are again arbitrary functions, and where we have an unspecified number of Wiener noise processes dW_i, as in Chapter 3.2. Solving this numerically is similar to solving the jump problem. We again define a function in the code that contains the deterministic part and another function that contains the stochastic part. The main difference here is just the syntax that we need to use. Let us define

$$x(0) = 10, \quad dx = -xdt + \frac{1}{1+|x|}dW_1 - \frac{1}{1+|x|}dW_2, \tag{6.4}$$

so that x seems to be constantly damping, until reaching small enough values where the noise terms start to be notable. Defining the deterministic part in code is only trivially different to the jump problem. The function that determines the stochastic part is defined in code as

```
function g(dx, x, p ,t)
    dx[1,1] = 1/(1 + abs(x[1]))
    dx[1,2] = -1/(1 + abs(x[1]))
end
```

where in `dx[i,j]` the `i` refers to the element of the vector which we are solving and `j` refers to the noise process. Once these are defined, defining the rest of the problem is easy

```
x_0 = [10.0]
tspan = (0.0, 10.0)
problem = SDEProblem(f, g, x_0, tspan,
                     noise_rate_prototype=zeros(1,2))
solution = solve(problem, Tsit5())
```

where there is one notable difference with the previous case, due to the use of `noise_rate_prototype=zeros(i,j)`, which is used so that the increment `dx` in function `g` has the proper shape. In the `noise_rate_prototype` the index `i` is the dimensions of the vector we are solving and the index `j` is the number of different noise processes. Since the noise prototype requires the dimensions of a vector it is not obvious how one might use this to solve matrices. This will be discussed in more detail in Chapter 6.4.3. The solution to Eq. (6.4) is plotted in Fig. 14.

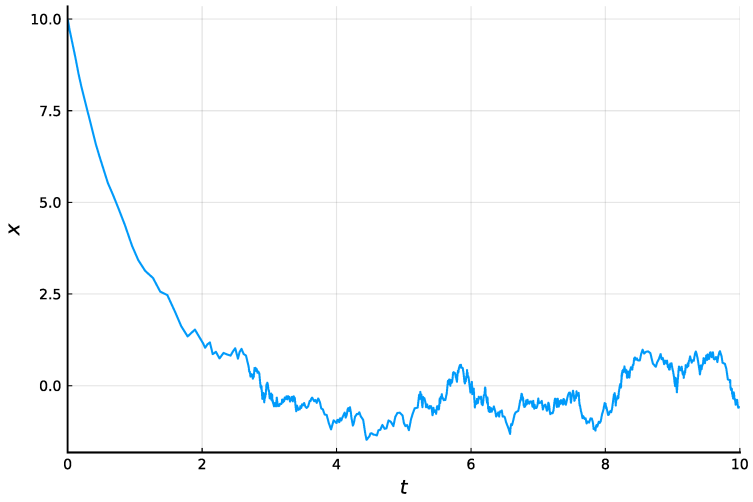

Figure 14: A numerically solved trajectory of Eq. (6.4). The value of x has been plotted as a function of time. Notice how x seems to get more noisy as it approaches zero.

6.2.3 Solving for Several Trajectories

Calculating several trajectories is simple with the differential equations package. This can be done by defining an `EnsembleProblem`, which takes as an argument the `problem`, which can be for example a `JumpProblem` or a `SDEProblem`, as in the previous examples. The argument `safetycopy=true` can be passed in the `EnsembleProblem` constructor, if you are also passing a `parameters` argument in the definition of the `problem`. With the `safetycopy=true` the program will make a copy of the `parameters` for each trajectory. Without this, all of the trajectories will access the same parameters, which can cause problems if the parameters are mutable (for example with pre-allocated matrices that are used to optimize calculation). To solve for `n` trajectories, `trajectories=n` needs to be written in the `solve` function.

6.2.4 Handling the Solution

The value of the time evolution at the time `t` is found by writing `solution(t)`. For times between the time steps there will be interpolation. To get the value at the `i`-th time step `solution[i]` can be used. Writing `solution.u` returns an array which contains the time evolution for specific time steps, which can be accessed from `sol.t`. The times between the time steps in `sol.t` are not

fixed by default. To store the time evolution at fixed time steps a `saveat=dt` parameter can be included in the `ODEProblem` or `SDEProblem` definition. I found it easiest to convert from the `solution` returned by the differential equations package to a simple array, which contains only the time evolution of the system, without the extra functionality found in the `solution` of the differential package. This conversion is somewhat unnecessary, since all the information is already contained in the `solution`, but I found this to be more intuitive to work with. For ensemble solutions the `solve` function will return an array of `solutions`. Since in quantum mechanics we are dealing with observables, we need to be able to calculate these from the numerically solved time evolution. This can be written conveniently as

```
result = [CalcObservable(psi, Args...) for psi in solution]
```

where the `solution` is an array containing the time evolution of the system. Ensemble solutions cannot be handled on a single line. In Julia functions can be passes as arguments to functions. To do this, in the function declaration the type of the argument needs to specified as a function. Here is an example for the syntax, and an idea for handling ensemble solutions

```
function CalculateMean(ensembleSolution,
                       CalcObservable::Function)
    #Calculate the mean over trajectories
end
```

The differential equations package provides several different solver algorithms. These have been compared in Fig. 15. There seems to be two different groups of solutions, but the reason for this or which group is the "correct" group was not found, thus the plots of this thesis should not be taken as exact results. The algorithm that was used for the plots of this thesis was the `SRA1` algorithm.

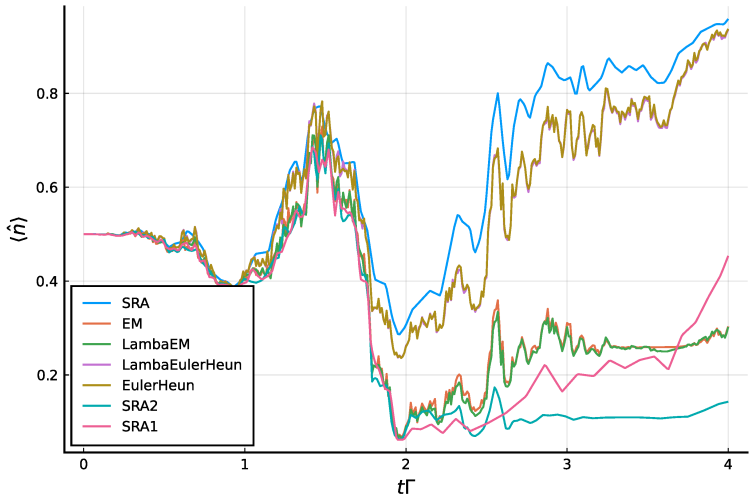

Figure 15: Comparison between some of the different solvers of the differential equations package. The equation solved is Eq. (6.5) for two transmons, for which the total boson number $\langle \hat{n} \rangle = \langle \hat{n}_1 \rangle + \langle \hat{n}_2 \rangle$ was calculated. The reason for the apparent two groups of solutions was not found. These were solved for two qubit transmons, with the parameters $\omega = U = J = \Gamma$ for the Bose-Hubbard Hamiltonian. The measurement operator was $\hat{n} \otimes \hat{I}$. Some of the solvers required a fixed time step, so these were all solved with a fixed time step $dt\Gamma = 0.01$. The initial state was $\hat{\rho}(0) = 1/2\left(|00\rangle\langle 00| + |01\rangle\langle 01|\right)$.

6.3 Optimization Performance in Julia

In this chapter some optimizing methods [31] that were used for numerically solving the continuous measurement problems are introduced. Optimizing comes down to reducing the number of allocations and the memory required to run the code. The `@time` and the `@code_warntype` macros can be used to investigate the performance of code.

The `@time` macro tells the execution time of a function together with the number of allocations and the number of bytes that were allocated when the function was executed. The `@time` macro is used by placing it in front of the function that is being executed:

```
@time result = CalculateSomething(args...)
```

There are many ways to reduce the number of allocations, but the the most notable tricks that were used for this thesis were the "dot syntax", which changes

the functions and operations to "vectorized" versions of them, and the other trick was to use pre-allocated vectors and matrices. The "dot syntax" allows Julia to combine computation to loops, which allows Julia to do the calculations without unnecessary allocation. The "dot syntax" changes the function and operations to perform element-wise. Here is an example on the "dot syntax":

```
result = s * v + s * m * v #Without dot syntax

result .= s . v .+ s .* m * v
```

where `s` is a scalar, `v` is a vector and `m` is a matrix. The second line on the example above is the preferred way to write that type of calculations. Notice that since the "dot syntax" changes the operations to be element-wise it cannot be used in matrix-vector or matrix-matrix multiplication. The "dot syntax" can also be used to do element-wise operations with functions, by writing `f.(args...)`. Note that the second line requires `result` to be defined before the calculation, so that `result` needs to be pre-allocated. Pre-allocation means that memory, that we know will be used in calculations, is reserved beforehand so that Julia does not need to do unnecessary temporary allocations, and due to this possibly unnecessary garbage collection. Here is an example on using pre-allocated matrices.

```
result = m1 * m2 #Without pre-allocations

result = zeros(2, 2) #Pre-allocating the matrix
mul!(result, m1, m2) #Calculating m1 * m2
```

Here `m1` and `m2` are some 2x2 matrices and `mul!` is a function that calculates the product of the two matrices and stores it in the matrix `result`. I found changing the matrix and vector products to pre-allocated versions of them with the `mul!` function had notable performance improvements.

The `@code_warntype` macro is used to make sure that functions do not have type instability. The compiler in Julia uses the types of the variables to generate machine code, so if there is ambiguity in the types of the variables, Julia will not be able to compile the code to machine code that is as efficient as it could be, i.e. type ambiguity leads to performance loss. The `@code_warntype` macro declares type instability with a red highlight in its output. The type instability issues are case dependant, the ones that I ran into were fixed by defining the types of the function arguments.

6.4 Numerically Solving the Continuous Measurement Problems

This chapter will provide the relevant parts of the code that was used to solve the continuous measurement problems. Before introducing the code, how to handle the parameters of the calculations is discussed. This chapter will conclude with a look on the performance of the code.

6.4.1 Handling All the Parameters

These numerical problems are dependant on several parameters. For example we have the number of transmons and the dimensions of one transmon or the dimension cut, since in practise we cannot have infinite matrices or vectors. We have the time span for which we are solving the time evolution. Then there are the parameters for the Hamiltonian, such as the coupling strength or anharmonicity. Dealing with all of them can be tedious. The parameters can be divided in to two groups: the ones that are necessary to define the problem and the ones that are necessary for the calculations. So for example we need to define the transmon transition frequency etc. to be able to define the Hamiltonian, but for the calculations we only need the Hamiltonian. The user should only be required to provide the parameters that are required to define the problem, and the parameters that are required for the calculations should be constructed from them. I found structs to be a good way to handle the parameters. Structs allow you to store different variables, but before the struct stores the variables it can process them, so that you can provide it with all the parameters required for the definition, and from them it will construct and store everything that is necessary for the calculations. There are also other benefits to using a struct. Using a parameters struct makes it easy to save the parameters in a file for note keeping, since all of the parameters are stored in one place. Julia's multiple dispatch can also be utilized to define alternative versions of functions that take the struct as an argument instead of the have parameters. This is convienient when writing the code, and when there are functions that depend on many parameters. Lastly, since we want to use pre-allocated matrices and vectors we need to store them somewhere to have access to them. In Julia, mutable structs can be used to store values that need to be change.

6.4.2 Numerically Solving Quantum Jumps

Let us take a look back at the photon detection of a two level atom, which was handled in example 3.1.1. For convenience the stochastic master equation is

repeated here

$$d\hat{\rho} = -\frac{i}{\hbar}[\hat{H}_{\mathrm{a}}, \hat{\rho}]dt - \frac{\Gamma}{2}\mathcal{H}\left[\hat{\sigma}^{\dagger}\hat{\sigma}\right]\hat{\rho}dt + \mathcal{J}\left[\hat{\sigma}\right]\hat{\rho}dN. \tag{3.23}$$

The rate of the jumps was given by

$$\left\langle \hat{\Omega}^{\dagger}\hat{\Omega} \right\rangle = \Gamma \left\langle \hat{\sigma}^{\dagger}\hat{\sigma} \right\rangle. \tag{3.22}$$

For a two level atom we know that after detecting a photon the atom has to be in its ground state. In code, these functions can be defined as

```
function f(drho, rho, p, t)
    dp .= (-1im * com(p.H, rho)
          - p.G / 2 * MSO(p.o' * p.o, rho))
end

rate(rho, p, t) = p.G * expVal(rho, p.o' * p.o)

affect!(integrator) = (integrator.u.u .=
                       [0.0im 0.0; 0.0 1.0])
```

where `p` denotes the struct containing the parameters needed for the calculation, with `p.G` $= \Gamma$ and `p.o` $= \hat{\sigma}$. The functions `com`, `MSO` and `expVal` calculate the commutator, apply the measurement superoperator $\mathcal{H}$ and calculate the expectation value respectively. The rest of the code is the same as in Chapter 6.2.1, with the difference that the parameters struct `p` is passed as an argument in the `ODEProblem` constructor after the time span. Note that in the code `p.o` is not used by itself, it is only used in the matrix `m = o' * o`, so it would have been a good idea to calculate and define the matrix `m` before hand in the struct and use it instead.

6.4.3 Numerically Solving Homodyne Detection

The stochastic differential equation that we are going to solve follows from Eq. (3.45), and is given by

$$d\hat{\rho} = -\frac{i}{\hbar}\left[\hat{H}, \hat{\rho}\right]dt + \sum_{j=1}^{n}\Gamma\mathcal{D}\left[\hat{\sigma}_j\right]\hat{\rho}dt + \sqrt{\Gamma}\mathcal{H}\left[\hat{\sigma}_j e^{i\phi}\right]\hat{\rho}dW_j, \tag{6.5}$$

where there are n different measurement operators. Here it is assumed that all the measurements have the same measurement rate Γ and phase ϕ. To account for multiple Wiener processes in the code we need to define

```
noise_rate_prototype = zeros(2 * d, n)
```

where d is the number of elements in the density operator. Due to the form of the noise_rate_prototype we need to be able to transform the density operator which is a complex matrix to an array of real numbers. Due to this transformation the number 2 appears in the definition of the noise_rate_prototype. The functions that I used to do these transformations are given here

```
#complex matrix -> real vector
function cmrv(m::Array{Complex{Float64},2})
    cvrv(vec(m))
end
#real vector -> complex matrix
function rvcm(v::Array{Float64,1}, dim::Int64)
    reshape(rvcv(v), dim, dim)
end
#complex vector -> real vector
function cvrv(v::Array{Complex{Float64},1})
    vcat(real(v),imag(v))
end
#real vector -> complex vector
function rvcv(v::Array{Float64,1})
    a = @view v[1:end÷2]
    b = @view v[(end÷2+1):end]
    a + 1im*b
end
```

These can be used to switch from complex matrices or complex vectors to an array of real numbers. With these tools and with the optimizing tricks in mind, we can write the code equivalent to Eq. (6.5). These are

```
function HomodyneDetection_f(drho, rho, p, t)
    #p.mPA[4] = rho, as a matrix
    p.mPA[4] .= rvcm(rho, p.dim)
    #Calculating [H, rho] with pre-allocated matrices
    p.mPA[5] .= -1im * com(p.H, p.mPA[4],
                 p.mPA[1], p.mPA[2])
    for o in p.meas
        #Applying the Lindblad superoperator
        p.mPA[5] .+= p.sp.G * LSO(o, p.mPA[4],
                     p.mPA[1], p.mPA[2], p.mPA[3])
```

```
    end
    #The increment is stored as an array of real numbers
    drho .= cmrv(p.mPA[5])
end

function HomodyneDetection_g(drho, rho, p, t)
    p.mPA[4] .= rvcm(rho, p.dim)
    #Looping over the measurement processes
    for (i,o) in enumerate(p.meas)
        p.mPA[1] .= sqrt(p.sp.G) * MSO(o*exp(1im * p.phi),
                    p.mPA[4], p.mPA[2], p.mPA[3])
        p.vPA .= cmrv(p.mPA[1])
        for j in 1:(2*p.dim)
            #Storing the stochastic part for
            #the i-th Wiener process
            drho[j,i] = p.vPA[j]
        end
    end
end
```

Here `p.mPA` is an array of pre-allocated matrices and similarly `p.vPA` is a pre-allocated vector. The function `LSO` applies the Lindblad superoperator. The pre-allocated matrix `p.mPA[4]` is used to store the density operator after transforming it back to a complex matrix. Pre-allocated versions of the functions `LSO` and `MSO` are used, hence the use of `p.mPA[1]`, `p.mPA[2]` and `p.mPA[3]`. The resulting increment of the density operator is stored in `p.mPA[5]` which is then transformed to a real array for the output. With these solving Eq. (6.5) numerically follows the example in Chapter 6.2.2 closely.

6.4.4 Numerically Solving Heterodyne Detection

The equation that we are solving is

$$d\hat{\rho} = -\frac{i}{\hbar}\left[\hat{H}, \hat{\rho}\right]dt + \sum_{j}^{n} \Gamma \mathcal{D}\left[\hat{\sigma}_j\right]\hat{\rho}dt + \sqrt{\Gamma}\mathcal{H}\left[\hat{\sigma}_j e^{it\Delta}\right]\hat{\rho}dW_j, \tag{6.6}$$

which follows from Eq. (3.70) similarly to Eq. (6.5) which was for homodyne measurement. The only difference is that the phase in the exponent is time dependant. Solving heterodyne detection numerically is exactly the same as for homodyne detection, with the exception that the time dependency has to be inserted in the function that handles the stochastic evolution. For handling the equations for transmons, where there are two noise processes for one measurement

operator, the dimensions of the `noise_rate_prototype` has to be changed so that the part dependant of the number of measurement operators is doubled. The function that I used for the stochastic part for transmons is

```
function TransmonsHeterodyneDetection_g(drho, rho, p, t)
    p.mPA[4] .= rvcm(rho, p.dim)
    for (i,o) in enumerate(p.meas)
        p.mPA[1] .= 0.5 * sqrt(p.G) * MSO(o, p.mPA[4],
        p.mPA[2], p.mPA[3])
        p.vPA .= cmrv(p.mPA[1])
        for j in 1:(2 * p.dim)
            drho[j, 2*i - 1] = p.vPA[j]
        end

        p.mPA[1] .= 0.5 * sqrt(p.G) * MSO(1im*o, p.mPA[4],
        p.mPA[2], p.mPA[3])
        p.vPA .= cmrv(p.mPA[1])
        for j in 1:(2 * p.dim)
            drho[j, 2*i] = p.vPA[j]
        end
    end
end
```

Here the two noise processes are handled in their own loops. Writing the code for the deterministic part is similar as it was for homodyne detection. For the stochastic Schrödinger equation (5.10), writing the code should not require any extra tricks that have not already been introduced, except that the stochastic Schrödinger equation does not conserve the norm so that the state vector has to be normalized in every time step. I did this by normalizing the state vector in the deterministic part, before using it to calculate the increment. It is possible that the differential equations package offers a better way to do this, but normalizing the state vector this way was sufficient.

6.4.5 Performance of the Numerical Solutions

To get a general picture on the size of the systems that are solvable with this code, we study the time it took to solve a single trajectory as a function of the size of the system. Fig. 16 depicts the solving time of the stochastic master equation Eq. (5.9), for different number of transmons n_T and for different single site dimensions d. For comparison, the same has been plotted for the stochastic Schrödinger equation Eq. (5.10) in Fig. 17. For these plots the calculation time

was solved only once so these results are volatile, and should be taken only as a general picture on the performance. These calculations were done on a personal computer with an AMD Ryzen™ 7 5800x CPU. The relevant parameters used that affect the calculating time are the time step $dtJ = 0.01$, the evolution time $tJ = 5$ and the tolerances $\mathrm{abstol} = \mathrm{reltol} = 10^{-3}$, which affect the accuracy of the result.

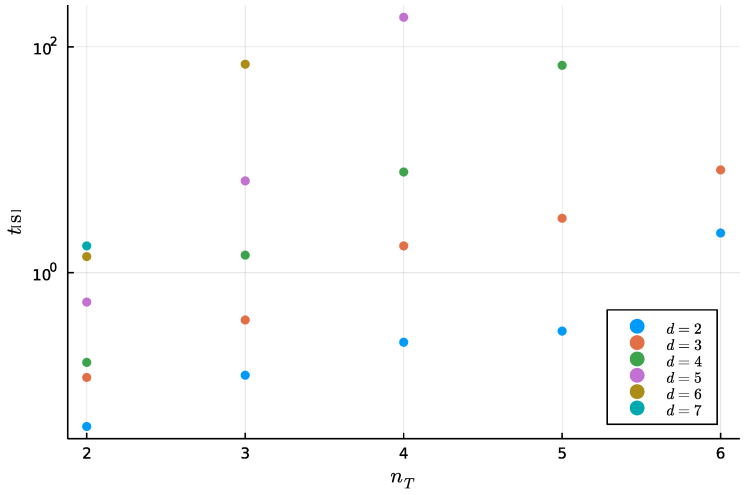

Figure 16: The time it took to solve a single trajectory of the stochastic master equation Eq. (5.9), plotted as a function of the number of transmons n_T for different dimensions of a single site d.

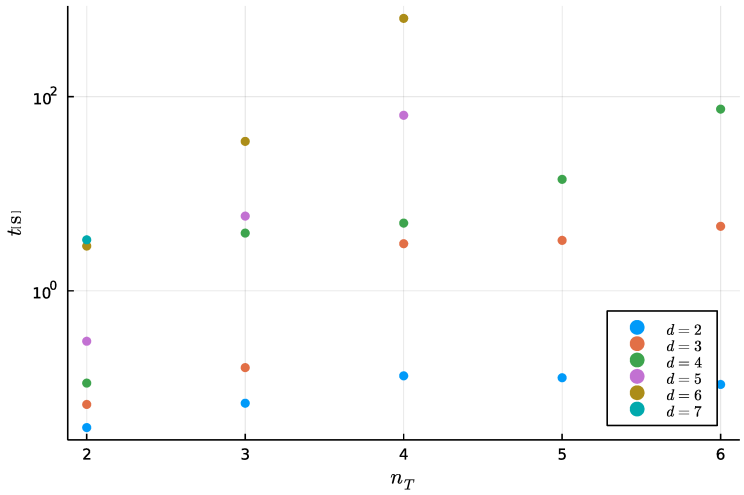

Figure 17: The time it took to solve a single trajectory of the stochastic Schrödinger equation Eq. (5.10), plotted as a function of the number of transmons n_T for different dimensions of a single site d.

7 Example Observables for Continuously Measured Transmons

This chapter demonstrates some results obtained from solving the time evolution for five transmons, where the boson number of the transmon in the center is being continuously measured. The equation solved numerically is

$$\begin{aligned} d\left|\Psi\right\rangle = &-\frac{i}{\hbar}\hat{H}_{\mathrm{BH}}\left|\Psi\right\rangle - \frac{\Gamma}{4}\hat{n}_3^2\left|\Psi\right\rangle dt + \frac{\Gamma}{4}\left\langle\hat{n}_3\right\rangle\hat{n}_3\left|\Psi\right\rangle dt - \frac{\Gamma}{8}\left\langle\hat{n}_3\right\rangle^2\left|\Psi\right\rangle dt \\ &+ \frac{\sqrt{\Gamma}}{2}\left(\hat{n}_3 - \left\langle\hat{n}_3\right\rangle\right)\left|\Psi\right\rangle dW_I - \frac{\sqrt{\Gamma}}{2}i\hat{n}_3\left|\Psi\right\rangle dW_Q,, \end{aligned} \tag{7.1}$$

which follows from Eq. (5.10). The Bose-Hubbard Hamiltonian Eq (4.4)

$$\hat{H}_{\mathrm{BH}}/\hbar = \sum_{i=1}^{5}\omega_i\hat{n}_i - \frac{U}{2}\sum_{i=1}^{5}\hat{n}_i\left(\hat{n}_i - 1\right) + J\sum_{i=1}^{4}\left(\hat{a}_i^\dagger\hat{a}_{i+1} + \hat{a}_{i+1}^\dagger\hat{a}_i\right). \tag{7.2}$$

describes the five transmons. The measurement operator is the boson number of the third site

$$\hat{n}_3 = I\otimes I\otimes\hat{n}\otimes I\otimes I, \tag{7.3}$$

where $\hat{n}$ is the number operator. The initial state was chosen to be

$$\left|\Psi(0)\right\rangle = \left|10101\right\rangle. \tag{7.4}$$

In the following chapters various observables have been plotted for the transmons that are described by Eq. (7.1). The observables have been plotted for different values of the measurement rate Γ. Single trajectories are shown together with the averaged result over one hundred trajectories. The parameters used in the calculations can be found in Table. 1.

We study two cases: identical transmons and disordered transmons [32]. The latter means that each transmon has its own transition frequency ω_i. The same quantities mentioned above have been calculated again for transmons with disorder. The distribution of the disorder is assumed to be uniform, meaning that the transition frequency of the i-th transmon is drawn from the interval $\omega_i = [-W, W]$ where W is the disorder amplitude. A specific set of ω_i is referred to as a realization of the disorder. For the plots with disorder, ten realizations were calculated with ten trajectories for every realization. For calculating the observable, first the ten trajectories for each realization were averaged to get an averaged density matrix, after this the observable was calculated, and the resulting values were averaged to end up with an average observable value over the realizations. In the plots without disorder, the average and the standard

deviation have been calculated over the trajectories. In the plots with disorder, the average and the standard deviation have been calculated over the realizations.

$\omega/2\pi$	1 MHz	t/J^{-1}	5
$U/2\pi$	250 MHz	dt/J^{-1}	0.01
$J/2\pi$	1 MHz	`abstol`	10^{-3}
n_T	5	`reltol`	10^{-3}
d_T	3		
$\hat{\sigma}$	$\hat{n}_3$	W/J	8 Mhz
$\|\Psi(0)\rangle$	$\|10101\rangle$	U_d/J	3.5 Mhz

Table 1: The parameters used for the results of this chapter. For the calculations five transmons where chosen, where each transmon has three possible states, hence $d_T = 3$. The `abstol` and `reltol` are parameters for the differential equation solver, which affect the accuracy of the solution. Anharmonicity of $U_\mathrm{d}/J = 3.5$ was used for the results with disorder $W/J = 8$. Other than these, the parameters are same for the results with and without disorder.

7.1 Boson Number of the Observed Site

Here the boson number of the site being measured has been plotted as a function of time. Single trajectories for different measurement rates are shown in Fig. 18a and in Fig. 19a, without and with disorder respectively. One hundred trajectories were calculated, and the average result together with the standard deviation is shown in Fig. 18b. The same has been plotted in Fig. 19b, but for ten trajectories per ten disorder realizations.

From Fig. 18a we see that when there is no measurement the excitations travel between the transmons, so that there is oscillation in the boson number $\langle \hat{n}_3 \rangle$. For $\Gamma/J = 1$ we can still see the oscillations, so that the measurement is weak and does not cause very significant back action on the system. For $\Gamma/J = 15$ the boson number is most of the time either at zero or at one, showing how the measurement dynamics dominate the time evolution. Since we are measuring the boson number, the strong measurement collapses the boson number to its eigenstates which can be seen in the boson number getting "stuck" at zero or one. In Fig. 18b we see that the oscillations remain for $\Gamma/J = 0$ and for $\Gamma/J = 1$. For $\Gamma/J = 15$ the boson number is on average around half bosons. This happens since the times at which the boson number is either at zero or one, as seen in Fig. 18a, do not happen at specific times. This is then seen as a average boson number of half, together with a large standard deviation.

For the plots with disorder, we see from Fig. 19a for $\Gamma/J = 0$ that the disorder

hinders the ability of the transmons to exchange excitations. Interestingly increasing the measurement rate seems to cause the transmon being measured to lose its excitation. Similar result is seen in Fig. 19b for the average over the realizations.

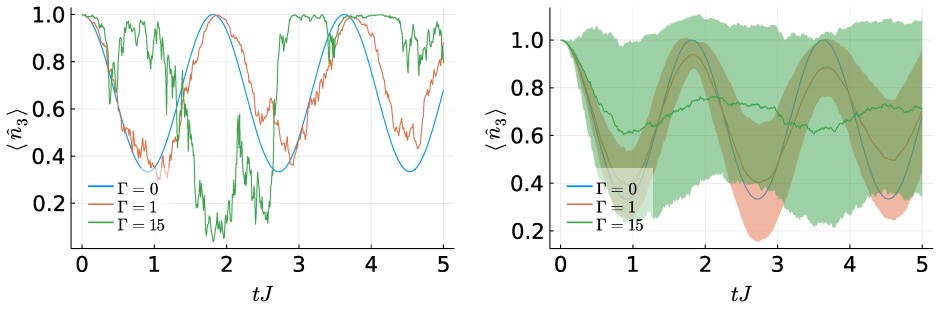

(a) (b)

Figure 18: The boson number of the site 3 being measured has been plotted as a function of time for $\Gamma/J = 0$ (blue), 1 (red) and 15 (green). Single trajectories are shown in panel (a). The averaged result over one hundred trajectories, where the width of the shaded area denotes the standard deviation, is shown in panel (b).

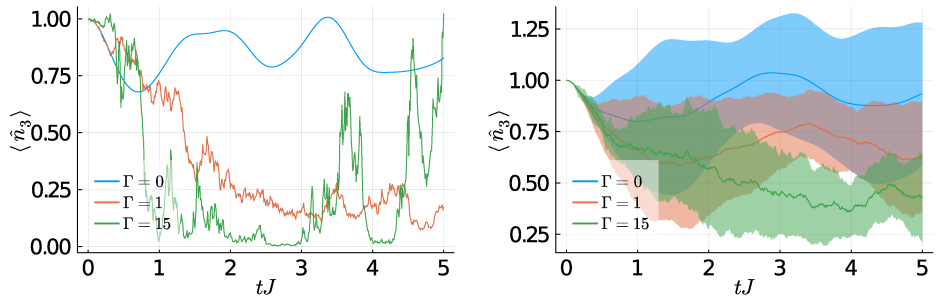

(a) (b)

Figure 19: The same as above but for disorder $W/J = 8$. The average and the standard deviation have been taken over the realizations.

7.2 Boson Number at the End of the Chain

Here the boson number of the last site has been plotted, so that we can see how does the measurement affect the transmons that are not under direct measurement. Similarly as before, single trajectories for different measurement

rates are shown in Fig. 20a and in Fig. 21a, without and with disorder respectively. One hundred trajectories were calculated, and the average result together with the standard deviation is shown in Fig. 20b. The same has been plotted in Fig. 21b, but for ten trajectories per ten disorder realizations.

Comparing to the plots on the boson number of the site being measured, we see that the measurement does not have as significant effect for the transmon at the end of the chain, even for $\Gamma/J = 15$. Still, the measurement does disturb the time evolution, which we see in Fig. 20a as a difference between the trajectories for different measurement rates. The evolution for the fifth transmon is not as jagged as for the transmon being measured, but the measurement does significantly change the overall evolution of the system. In the averaged results in Fig. 20b, we still see the oscillation of the boson number, even for $\Gamma/J = 15$.

As seen in Fig. 19a the measurement can cause the transmon being measured to lose its excitation. This can be seen in Fig. 21a, where the boson number of the fifth site has increased for $\Gamma/J = 1$. In Fig. 21b on average the measurement reduces the oscillation of the boson number. Interestingly for $\Gamma/J = 1$ the average boson number seems to be larger than for $\Gamma/J = 0$ or $\Gamma/J = 15$, suggesting that there exists a value of Γ for which the boson number of the fifth site the greatest.

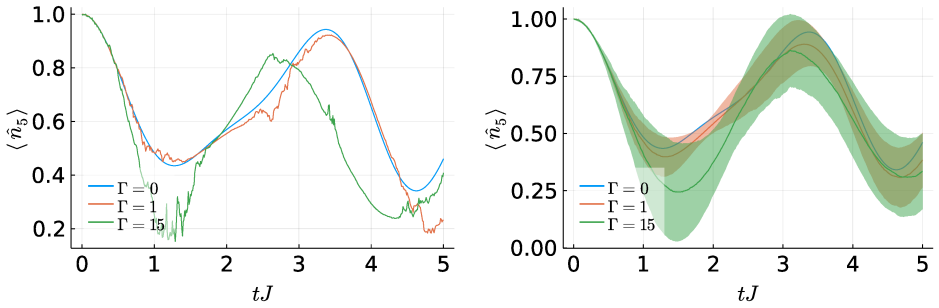

(a) (b)

Figure 20: The boson number of the fifth transmon has been plotted as a function of time for $\Gamma/J = 0$ (blue), 1 (red) and 15 (green). Single trajectories are shown in panel (a). The averaged result over one hundred trajectories, where the width of the shaded area denotes the standard deviation, is shown in panel (b).

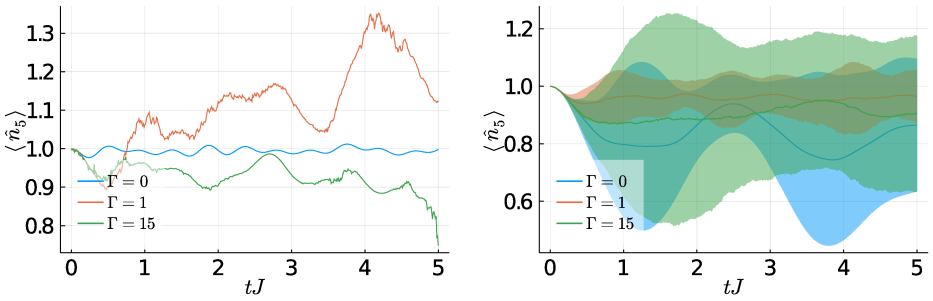

(a) (b)

Figure 21: The same as above but for disorder $W/J = 8$. The average and the standard deviation have been taken over the realizations.

7.3 Entanglement Entropy

We can divide the chain of transmons into two parts. The first part consists of the first two transmons and the second of the rest. We can calculate the entanglement [32] between these two parts by calculating the von Neumann entropy

$$S = -\mathrm{Tr}_{12}(\hat{\rho}_{12} \ln \hat{\rho}_{12}), \tag{7.5}$$

where $\hat{\rho}_{12}$ is the density matrix describing the first two transmons, which can be calculated by tracing out the third, fourth and the fifth transmon. Here Tr_{12} is the trace over the basis states of the density operator that describes the first two transmons. The entanglement has been plotted without disorder in Fig. 22a and Fig. 22b. The result with disorder is shown in Fig. 23a and Fig. 23b. The number of trajectories used and the number of realizations is the same as before.

Similarly as in Fig. 18a, we see in Fig. 22a how the Bose-Hubbard Hamiltonian naturally generates oscillating entanglement. The oscillations are still apparent with $\Gamma = 1/\mathrm{J}$, but with $\Gamma = 15/J$ they are reduced, which can be seen well in Fig. 22b. The averaged entanglement for $\Gamma = 15$ seems to be approaching a steady state, but this should be investigated further by plotting for a longer period.

In Fig. 23b we see that the measurement increases the entanglement of the system. It would be interesting to see if the entanglement plateaus for some value of the measurement rate, and what that value would be and the corresponding maximum entanglement.

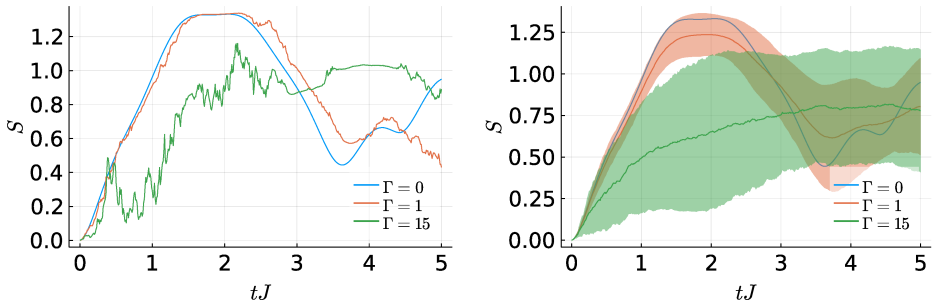

(a) (b)

Figure 22: The entanglement entropy S of Eq. (7.5) has been plotted as a function of time for $\Gamma = 0/J$ (blue), 1 (red) and 15 (green). Single trajectories are shown in panel (a). The averaged result over one hundred trajectories, where the width of the shaded area denotes the standard deviation, is shown in panel (b).

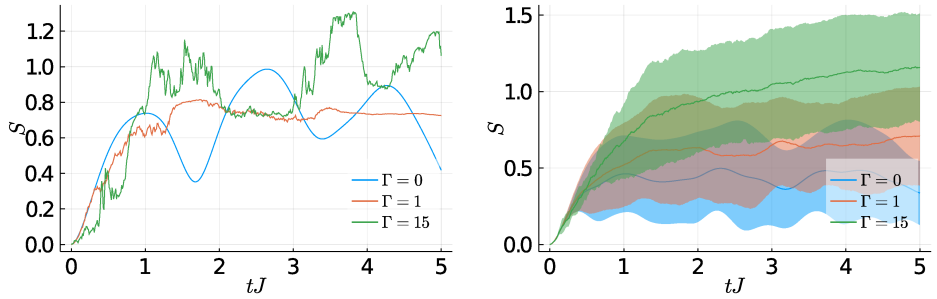

(a) (b)

Figure 23: The same as above but for disorder $W/J = 8$. The average and the standard deviation have been taken over the realizations.

7.4 Accuracy of the Results

To make sure the numerical program functions as it should, Eq. (7.1) was solved for two transmons with the Bose-Hubbard Hamiltonian parameters of $\omega = U = 0$ and $J = \pi$. Plotting this showed the boson number oscillating between the transmons, with a period of $tJ = 1$. For the stochastic Schrödinger equation the norm of the wave function should be conserved, and for the stochastic master equations the conserved quantity is the trace of the density matrix. Both of these were tested and deemed conserving, but with some deviation due to the numerical nature of the calculation. The tolerances `abstol` and `reltol` affected

how much the norm and the trace varied. They were chosen so that the general nature of the time evolution can be seen, without the calculation becoming too time consuming. Since the results here are only meant to be indicative, the tolerances do not need to be strict. Additionally, the boson number should be conserved for Eq. (7.1) and indeed it does, with similar volatility as the norm.

For these calculations I found one hundred trajectories to be sufficient to get a general picture of the time evolution, while being sufficiently fast to calculate. For the results with disorder, ten realizations with ten trajectories is not much. It would be interesting to investigate how the results change with more realizations, but since for every realization there has to be a set number of trajectories, the calculation becomes very slow very quickly.

The cut of the single transmon dimension was chosen to be $d_T = 3$, allowing states $|0\rangle$, $|1\rangle$ and $|2\rangle$ for a transmon. The truncation was needed, since otherwise the calculation would have taken too much time. Since the initial state is $|\Psi(0)\rangle = |10101\rangle$ in total we have three bosons, so that the state $|3\rangle$ is possible for a single transmon. Due to this the cut does affect the evolution, since it removes otherwise possible states from the basis. But, as we see from Fig. 18b and Fig. 20b, the boson number does not significantly go above one, so the cut should not have a major effect on the time evolution.

For single trajectories, decreasing the time step does not seem to change the overall picture. Nevertheless, since the calculation becomes heavy when the time step is decreased, the effect of changing the time step on the average results was not investigated.

Lastly, there is the question on the validity of the solver algorithm, as in Chapter 6.2.4. Since it was not found that if the solver algorithm for stochastic differential equations used is somehow not suitable for these calculations, then the results here can be quite unreliable. Definitely for more accurate results, which go beyond this thesis, the solver accuracy should be thoroughly investigated, and even for the results here, the correctness of the solver should have been figured out.

8 Conclusions

The basics of measurement theory were introduced to provide basis for studying continuous measurement. The stochastic master equations for quantum jumps, homodyne and heterodyne detection were derived in the context of optical quantum mechanics, and the behaviour of these equations were demonstrated graphically and conceptually. To bridge the gap to superconducting circuits, superconductivity and the transmon device were introduced, followed by the Bose-Hubbard model to understand how an array of transmons can be modeled. What in practise is required on a superconducting circuit to measure transmons was explained, by introducing the superconducting cavity as a key to probe and control the transmons. Finally, the stochastic master equation, and the stochastic Schrödinger equation, for the heterodyne measurement of transmons was introduced, concluding the theory of this thesis.

The theory was tested numerically by solving the equations modeling the continuous measurement of a transmon array with the differential equations package found in Julia. The capabilities of Julia for numerically solving continuous measurement problems were investigated, with the conclusion that Julia is an efficient language, and when paired with the differential equations package provides an easy way to solve various stochastic differential equations. The performance of the written numerical program was tested, with the results suggesting that the numerical solving of the stochastic Schrödinger equation could be further optimized. Some observables were calculated and shown, to further demonstrate the capabilities of the code written to solve the stochastic Schrödinger equation relating to the heterodyne measurement of transmons. With a personal computer, one hundred trajectories for five transmons with a dimension cut of $d_T = 3$ are easily calculable.

There are several ways to expand this thesis. Since the details of the derivation of the transmon specific stochastic differential equations were left out, to further developed understanding of continuous measurement with superconducting circuits these details could be investigated. The numerical program works, but better optimization is possible. Significant speed up could be achieved by reducing the size of the matrices and vectors used in the calculations. This could be done by using sparse matrices. Another approach is to change the program to work in a reduced basis where there are only states with equal number of boson, since for the stochastic Schrödinger equation used here the boson number is conserved. This would enable the study of larger systems, and the use of more trajectories and realizations. The results could be further analyzed, and the program could be used to further study the details of the observables studied in the previous chapter. Nevertheless, the absolute first step should be to figure out which solver should be used for these types of calculations.

References

[1] G. Wendin, *Quantum Information Processing With Superconducting Circuits: a Review*, Rep. Prob. Phys. **80** 106001 (2017).

[2] S. Hacohen-Gourgy, & L. S. Martin, *Continuous Measurement for Control Of Superconducting Quantum Circuits*, Advances in Physics: X, 5:1 (2020).

[3] D. J. Griffiths, *Introduction to Quantum Mechanics*, (Prentice Hall, Upper Saddle River, 1995).

[4] J. A. Wheeler, & W. H. Zurek, *Quantum Theory and Measurement*, (Princeton, New Jersey, Princeton University Press, 1983).

[5] K. Jacobs, *Quantum Measurement Theory and Its Applications*, (Cambridge, UK, Cambridge University Press, 2014).

[6] T. A. Brun, *A Simple Model of Quantum Trajectories*, Am. J. Phys. **70**, 719 (2002).

[7] H. M. Wiseman, & G. J. Milburn, *Quantum Measurement and Control*, (Cambridge, UK, Cambridge University Press, 2010).

[8] D. A. Steck, *Quantum and Atom Optics*, available online at http://steck.us/teaching (revision 0.13.2, 20 May 2020).

[9] K. Jacobs, *Stochastic Processes for Physicists : Understanding Noisy Systems*, (Cambridge, UK, Cambridge University Press, 2010).

[10] J. Clarke & F. K. Wilhelm, *Superconducting Quantum Bits*, Nature **453**, 1031–1042 (2008).

[11] J. Koch et al. *Charge-Insensitive Qubit Design Derived From the Cooper Pair Box*, Phys. Rev. A **76**, 042319 (2007).

[12] https://www.ibm.com/quantum-computing.

[13] S. Sachdev, *Quantum Phase Transitions*, (Cambridge: Cambridge University Press, 2011. v. 2nd ed).

[14] N. K. Langford, *Circuit QED — Lecture Notes*, arXiv:1310.1897v1 (2013).

[15] T. E. Roth et al., *An Introduction to the Transmon Qubit for Electromagnetic Engineers*, arXiv:2106.11352v1 (2021).

[16] T. Orell et al., *Collective Bosonic Effects in an Array of Transmon Devices*, Phys. Rev. A **105**, 063701 (2022).

[17] A. Blais et al., *Quantum Information Processing With Circuit Quantum Electrodynamics*, Phys. Rev. A **75**, 032329 (2007).

[18] A. A. Clerk et al., *Introduction to Quantum Noise, Measurement and Amplification*, Rev. Mod. Phys. **82**, 1155 (2010).

[19] M. Silveri et al., *Theory of Remote Entanglement via Quantum-Limited Phase-Preserving Amplification*, Phys. Rev. A **93**, 062310 (2016).

[20] A. Blais et al., *Cavity Quantum Electrodynamics for Superconducting Electrical Circuits: An Architecture for Quantum Computation*, Phys. Rev. A **69**, 062320 (2004).

[21] A. Wallraff et al., *Strong Coupling of a Single Photon to a Superconducting Qubit Using Circuit Quantum Electrodynamics*, Nature **431**, 162-167 (2004)

[22] M. A. Nielsen, & I. L. Chuang, *Quantum Computation and Quantum Information: 10th Anniversary Edition*, (Cambridge, UK, Cambridge University Press, 2010).

[23] C. M. Caves et al., *Quantum Limits on Phase-Preserving Linear Amplifiers*, Phys. Rev. A **86**, 063802 (2012)

[24] N. Bergeal et al., *Phase-Preserving Amplification Near the Quantum Limit With a Josephson Ring Modulator*, Nature **465,** 64-68 (2010)

[25] M. Hatridge et al., *Quantum Back-Action of an Individual Variable-Strength Measurement*, Science **339**, 178-181 (2013).

[26] https://julialang.org/

[27] https://julialang.org/blog/2012/02/why-we-created-julia/

[28] C. Rackauckas, http://www.stochasticlifestyle.com/7-julia-gotchas-handle/

[29] https://julialang.org/benchmarks/

[30] https://diffeq.sciml.ai/stable/

[31] https://docs.julialang.org/en/v1/manual/performance-tips/

[32] T. Orell et al., *Probing the Many-Body Localization Phase Transition with Superconducting Circuits*, Phys. Rev. B **100**, 134504 (2019).